



TECHNISCHE
UNIVERSITÄT
WIEN

Vienna University of Technology

MASTERARBEIT

A High-resolution Diffuse Fraction Model for Vienna

ausgeführt zum Zwecke der Erlangung des akademischen Grades
einer **Diplom-Ingenieurin**

unter der Leitung von
Univ.-Prof. Dipl.-Ing. Dr.techn. Ardeshir Mahdavi
E 259-3 Abteilung für Bauphysik und Bauökologie
Institut für Architekturwissenschaften

eingereicht an der
Technischen Universität Wien
Fakultät für Architektur und Raumplanung

von
Ehsan Mahmoudzadeh Vazifeh

Matrikelnr. 1227658
Erdbergstraße 220/6/3, 1110, Wien

Wien, im Januar 2014

Kurzfassung

Für thermische und visuelle Simulationen, sind exakte Kenntnisse der direkten und diffusen Komponenten der Sonneneinstrahlung welche auf eine absorbierende Oberfläche treffen, notwendig. Zuverlässige und präzise Sensoren zur Messung der Strahldichteverteilung des Himmelsgewölbes sind sehr kostenintensiv. Aber es wird weltweit an vielen Orten mit einfacheren Messinstrumenten die horizontale Globalstrahlung erfasst. Daher wurde in einigen wissenschaftlichen Veröffentlichungen die Vorhersage von genauerer Daten zur Solarstrahlung basierend auf einfachen Strahlungsmessungen untersucht. Es wurden bereits einige Versuche, horizontale Globalstrahlung in direkte und diffuse Komponenten zu zerlegen, von verschiedenen Autoren vorgestellt. Aktuelle Studien (Dervishi und Mahdavi, 2012 and Vazifeh et al., 2013) zeigen die Schwächen der bestehenden Modelle basierend auf Daten, die an der TU-Wien gesammelt wurden. In der vorliegenden Arbeit werden verschiedene Vorhersagemodelle untersucht und evaluiert, und ein neuer Ansatz für das von der TU entwickelte Model wird vorgeschlagen. Des Weiteren wird ein Verfahren zur Generierung eines Modells für die diffusen Anteile der Sonnenstrahlung vorgestellt. Zusätzlich wird ein Verfahren zur Berechnung von Himmelstrahlung für wolkenlosen klaren Himmel unter Verwendung einer linearen kleinstes Quadrat Regression gezeigt.

Summary

Direct and diffuse components of solar radiation reaching to the collecting surfaces must be known, for building thermal and visual simulation. High accuracy sensors to measure sky dome radiance distribution are very expensive. However, simple measurements of global horizontal radiation are widely performed for many locations around the world. Consequently, prediction of more accurate solar radiation data based on simple irradiation measurements was addressed in several studies.

Several attempts to split global horizontal irradiance to direct and diffuse components have been done by numerous authors. Recent studies by Dervishi and Mahdavi (2012) and Vazifeh et al. (2013) showed the shortcoming of the existing models using data collected from the weather station of Building physics and Building ecology department, Vienna University of Technology. In this thesis the performance of a number of well-known diffuse or direct fraction prediction models were evaluated and a new model for the location of Vienna, Austria was proposed. Moreover, a new approach to generate a global diffuse fraction model was presented.

In addition, a sky radiance distribution model for the cloudless sky was developed using linear least square regression.

Keywords

Diffuse fraction, global horizontal radiation, clearness index, solar altitude, Radiance coefficient.

Acknowledgments

Primarily, I would like to give my boundless gratitude to Professor Mahdavi for his constant encouragement and great support. This work would not have been possible without his remarkable suggestions, patience and dedication of his time.

I would like to give my sincere thanks to Dr. Matthias Schuß, for sharing his tremendous knowledge and support through my whole period of study.

I also would like to thank my colleagues in the department of Building physics and Building ecology for their supportive spirits.

At the end I want to send my gratitude to my lovely family, my uncle, and my grandmother, especially my mother for her endless love.

for Farah

Contents

Kurzfassung	II
Summary	III
Acknowledgments	IV
<i>for Farah</i>	V
Chapter 1 Introduction	1
1.1 Background.....	3
1.2 Motivation	4
Chapter 2 Dataset	5
2.1 Data quality control and comparison	6
Chapter 3 Models description	7
3.1 Diffuse fraction models	7
3.1.1 Polynomial models.....	7
3.1.2 Logistic function models	14
3.1.3 Exponential Models	15
3.1.4 Development of a new hourly Model for Vienna	18
3.2 Radiance distribution model	26
Chapter 4 Results & Discussions	31
4.1 Model performances	31
4.1.1 Erbs et al.	31
4.1.2 Reindl et al.	32
4.1.3 Skartveit and Olseth.....	33
4.1.4 Boland et al.	34
4.1.5 Boland-Ridley-Lauret	34
4.1.6 Maxwell.....	35
4.1.7 Perez	35

4.1.8	New Model for Vienna	36
4.2	Models performance evaluation	37
4.3	Seasonal and solar impact	41
4.4	Diffuse model verification.....	43
4.5	Radiance model performance	44
Chapter 5	Conclusions and Outlook	51
5.1	Diffuse fraction models	51
5.2	Radiance distribution model	51
Chapter 6	References.....	52
6.1	Literature.....	52
6.2	Tables	55
6.3	Figures.....	56
Appendix A:	Weather Station	58
Appendix B:	The ratio of hourly global horizontal radiation to hourly extraterrestrial radiation	62
Appendix C:	Perez look-up table.....	65
Appendix D:	Irradiance distribution sheets	72

Chapter 1

Introduction

Energy is ubiquitous in our everyday life. Its main sources are fuel and electricity. Electricity is being produced by renewable and non-renewable energy sources. Non-renewable energy sources which cannot be replenished are comprised from fossil fuels (e.g. coal, oil, lignite, nuclear) and renewables are represented by wind, solar panels, geothermal, biomass, hydropower, etc. Energy is being used in transportation, industry, services, agricultures, and households sectors. Moreover, buildings consume around 40% of total final energy consumption in Europe (Lapillonne et al. 2012).

Figure 1-1, illustrates energy consumption by different parts of the Residential sectors. Approximately 72% of it is used for HVAC and lighting system. Due to this fact, enhancing the building performance will significantly decrease the energy consumption of the buildings. Solar energy, in form of photovoltaic or solar thermal collectors, can be used as a renewable energy to decrease the dependency of buildings to fossil energy. Solar radiation data is of high importance for applications in thermal and visual building simulation. Design of solar systems (sizing, orientation), fenestration and shading, control and automation of HVAC and lighting system is significantly influenced by the amount

Introduction

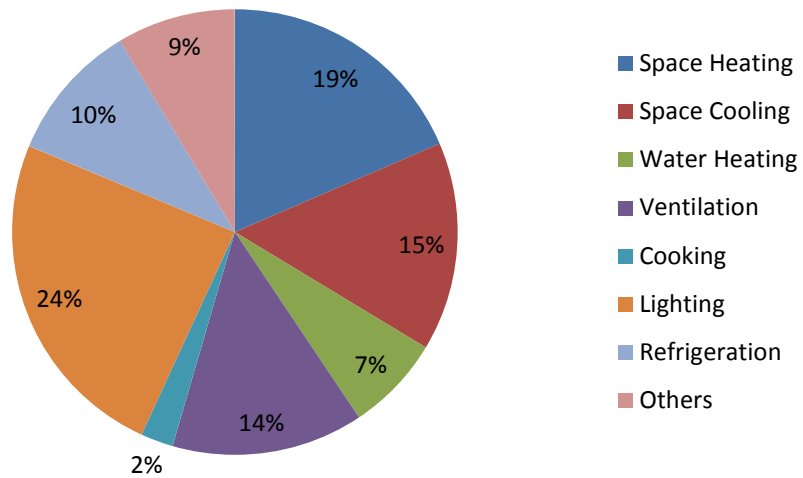


Figure 1-1. Typical energy usage of commercial buildings profile (U.S energy information administration)

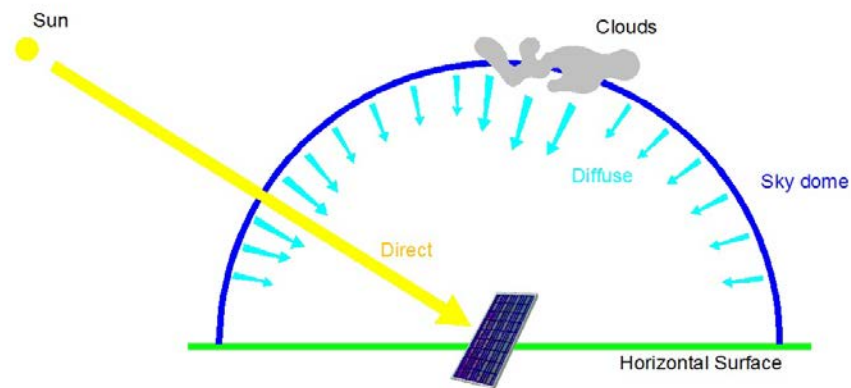


Figure 1-2. Depiction of direct and diffuse component of solar insolation

of solar radiation reaching to the building. On the other hand, light can influence the efficiency and productivity, wakefulness, sleep and mood of people throughout the day. Scientific Committee on Emerging and Newly Identified Health Risks elaborated on health effects of artificial light and indicated high risk of health damage by using artificial light (SCENIHR 2012). In order to obtain a full benefit of daylight and avoid overheating, optimization of design strategies for building geometry is necessary.

Solar radiation, reaching the collecting surfaces, consists of two components, a) direct or beam radiation from the sun disc, b) diffuse radiation, or incident

Introduction

radiation, scattered or absorbed in the atmosphere by dust, gas, water vapour etc. or reflected by clouds. Sum of these two on a horizontal surface will result into the global horizontal irradiance (See *Figure 1-2*). Diffuse solar radiation is anisotropic over the sky dome, which makes calculation of diffuse radiation on a tilted surface relatively complicated. Thus, amount of diffuse radiation and its distribution throughout the sky dome is crucial. Due to the high cost of instruments for radiation measurement, most of weather stations provide only global horizontal radiation data. This fact has motivated scientists to calculate direct and diffuse component of solar radiation from the global horizontal radiation.

1.1 Background

Previous works aiming to predict solar components were done in 1954 by Parmerlee 1954, who considered only clear sky condition. After him, Liu and Jordan 1960 studied both cloudy and clear sky condition. Most of the data, used in their works, is based on hourly values up to average daily or monthly values. Later, Erbs 1982, used 'hourly k_t , the ratio of hourly global horizontal radiation to hourly extra-terrestrial radiation' in a piecewise function for predicting the diffuse fraction. Iqbal 1980 and Skartveit and Olseth 1998 added solar elevation as a variable, in addition to hourly clearness index k_t . In 1988, Davies et al. evaluated the performance of 12 solar irradiance models (including Erbs et al. 1982 and Orgill and Hollands 1977) as a part of international collaborative study of the IEA's solar heating & cooling program. Data was based on hourly to monthly values and different seasons of 7 countries, namely Australia, Canada, Netherlands, Switzerland, United Kingdom, USA and West Germany. Davies concluded that diffuse fraction model of Erbs et al. 1982 performs better than other models. Later, Reindl et al. 1990 reduced a set of 28 potential variables down to 4 important variables by using stepwise regression. These variables included namely clearness index, solar elevation, temperature, and relative humidity. In another study with data sets from France, Netherland, Switzerland and USA, (Perez, 1990) concluded that (Maxwell, 1987) DISC model performs better than two models of Erbs et al. 1982 and Skartveit and Olseth 1998. The Maxwell 1987 DISC model requires hourly clearness index and air mass as inputs, which are solar elevation dependent. In his first model Perez et al. 1991 added a coefficient to Maxwell

Introduction

beam irradiation model (DISC), comprised of four insolation conditions parameters. This coefficient involves a four-dimensional look-up table.

1.2 Motivation

The accurate prediction of building energy performance is necessary for decreasing the lifetime energy consumption of a building. It is especially a vital issue nowadays, due to a global rise of energy prices. There are several uncertainties in a building simulation, i.e. assumptions of building loads, loads by human activity, occupancy prediction and building geometry and construction modeling. These ambiguities can lead to poor and unreliable result of the simulation. Amount of solar radiation, reaching the building surface, must be known for thermal and lighting building simulation purposes. extensive studies have been done in the past to investigate the impacts of various variables on the variation of solar radiation components. Numerous researchers have chosen different variables such as clearness index, solar altitude, temperature, air mass, relative humidity etc., but presented their model mostly by clearness index. Those studies are limited to local or similar climate application. Recent studies (Dervishi and Mahdavi 2012) and (Vazifeh et al. 2013) showed that none of those models perform satisfactorily for the location of Vienna, Austria. Data used in this thesis is discussed in Chapter 2. In Chapter 3, rigorous revision of those models is done, performance of the models and their vulnerability is evaluated with an aim of predicting the diffuse component of solar irradiance. Moreover, approach has been given to predict the solar components. Besides, a simple model is proposed, which appears to perform better than other mentioned models for the location of Vienna, Austria. Evaluation of model performance is demonstrated and discussed in Chapter 4.

Chapter 2

Dataset

For this thesis, data was collected from the Department of Building Physics and Building Ecology weather station (BPI), located on the rooftop of the tower of TU WIEN, at the heart of Vienna ($48^{\circ}11'55''\text{N}$, $16^{\circ}22'10''\text{E}$), it is equipped with accurate measuring instruments. The specification of these instruments can be found in Appendix A. Other data is taken from Hohe-Warte weather station, which is the main weather station of the Austrian weather service ($48^{\circ}14'56''\text{N}$, $16^{\circ}21'26''\text{E}$) (See *Figure 2-1*). Vienna is located in a mid-oceanic and humid continental climate, according to the Köppen classification, 200 m height above sea level. The climate is typically cloudy, moderately cold winters, sunny and hot summers with relatively high wind speed. (See Appendix I for recorded climate data for Vienna from 1971 to 2000).

Data sets for the year 2011 and 2012 were used from both stations under all weather conditions. At BPI station, two sensors were used for measuring global horizontal radiation (Kipp & Zonen CM3, Delta-T SPN1) and two other sensors for measuring diffuse horizontal radiation (Delta-T SPN1, Skyscanner [MS321LR]). The CM3 pyranometer consists of a thermopile sensor, a housing, a dome, and a cable.



a) Building physics weather station



b) Hohe-Warte weather station (Source: www.zamg.ac.at)

Figure 2-1. Weather station overview

Dataset

The high quality thermopile has a black absorbent coating. The coating absorbs the radiation and converts it to heat. Dome protects thermopile against moisture and other external influences. The SPN1 Sunshine pyranometer measures the direct and diffuse components of the global solar radiation, using seven miniature thermopile sensors plus a computer-generated shading pattern. The diffuse horizontal radiation is also calculated by sky scanner, which divides the sky dome into 145 patches and measures two values of radiance and luminance for each patch.

2.1 Data quality control and comparison

Data quality plays an important role in data analysis and model development. To achieve a reliable and trustful level of data, several steps of rigorous quality control analysis has been done to the BPI data, which are:

- 1) The comparison of global horizontal irradiance data from sunshine pyranometer (Delta-T SPN1) with an accurate Pyranometer (Kipp & Zonen CM3) and elimination of data, with more than 5% of deviation for the whole period of the measurement.
- 2) Discarding the data with solar altitude of less than 5 degree, due to the possibility of obstructed sun by the surrounding hills.
- 3) Elimination of data with global horizontal radiance less than 50 watts per square meters or clearness index of higher than unit.

Chapter 3

Models description

3.1 Diffuse fraction models

Many models were developed with the aim of decomposition of global solar radiation into direct and diffuse part. In this chapter, three different categories of models have been discussed, depending on their function. *Table 3-1*, summarizes the models function type and their variables. The models have been implemented in the Matlab programming environment. All the models require solar altitude to be calculated for each hour. Calculation of solar altitude has been taken from the NREL (National Renewable Energy Laboratory) official web page.

3.1.1 Polynomial models

Several simple polynomial models were developed in order to derive diffuse component of solar radiation. Liu and Jordan 1960 developed a linear function based on k_t , the hourly global horizontal radiation to the hourly extraterrestrial radiation.

$$k_t = \frac{I_{Global}}{I_{extraterrestrial} \times \sin \alpha} \quad (1)$$

Table 3-1. brief summary of models and their input variables

Models	Abbreviation	Function	Input variables
Erbs et al. 1982	EKDH	Polynomial	k_t
Reindl et al. 1990	RBDH	Polynomial	$k_t, \sin \alpha, T_a, \phi$
Skartveit and Olseth 98	SKOH	Polynomial	k_t, α, σ_3
Boland et al. 2001	BOLH	Logistic	k_t
Lauret et al. 2010	BRLH	Logistic	$k_t, AST, \alpha, K_t, \varphi$
Maxwell 1987	MAXH	Exponential	k_t, m_{air}
Perez et al. 1991	PERH	Exponential	$k_t, m_{air}, W, \vartheta_z, k'_t,$

Models description

$$k_d = \frac{I_{Diffuse}}{I_{Global}} \quad (2)$$

$$I_{extraterrestrial} = 1367 \left(1 + 0.33 \cos \frac{360n}{365} \right) \quad (3)$$

Orgill and Hollands 1977 proposed a diffuse fraction model with the same input (k_t), using data from Toronto, Canada. Subsequently, Iqbal 1980 and Skartveit and Olseth 1998 used, in addition to k_t , the solar altitude as a second important variable, with dataset of locations in Canada and France. This model showed a significant improvement in the accuracy of the results.

Reindl et al. 1990 derived new diffuse fraction correlations by using 4 variables namely clearness index k_t , solar altitude α , temperature and relative humidity, which could decrease standard errors by 26 %, with Erbs et al. 1982 correlation.

3.1.1.1 Erbs et al.

Erbs et al. 1982 indicated the disagreement of hourly, daily, monthly relationships in estimation of diffuse fraction, depending on the purpose of use of the diffuse correlation. Consequently, he tried to develop relationships for estimation of diffuse fraction from hourly, daily, and monthly-average global radiation and comparison of them with existing relationships for different seasons. In this thesis, hourly diffuse fraction correlation is used.

Data sets were used from pyranometer and pyrhelimeter of four locations in the United States in order to derive correlation between k_t and diffuse fraction. Diffuse fraction was described as below:

For $k_t \leq 0.22$;

$$\frac{I_d}{I} = 1 - 0.09k_t \quad (4)$$

For $0.22 \leq k_t \leq 0.8$

$$\frac{I_d}{I} = 0.9511 - 0.1604k_t + 4.39k_t^2 - 16.64k_t^3 + 12.34k_t^4 \quad (5)$$

For $k_t > 0.8$;

Models description

$$\frac{I_d}{I} = 0.165 \quad (6)$$

For k_t more than 0.8, Erbs applied a constant value for diffuse fraction, using the same approach as Orgill and Hollands 1977. They noticed that for this range of k_t amount of diffuse fraction increases due to the phenomenon of unobstructed sun and partly cloudy sky.

3.1.1.2 Reindl et al.

Reindl et al. 1990 developed new diffuse fraction correlations based on the idea that commonly measured climatic variables should be used as predictors. They used a function with 4 variables of k_t , solar altitude α , temperature and relative humidity for comparison of former Liu and Jordan type correlation using 22000 hours of measurements from five stations around Europe and United States. Finally they developed three correlations, which are:

For $k_t \leq 0.3$; $\frac{I_d}{I} \leq 1.0$

$$\frac{I_d}{I} = 1.00 - 0.232k_t + 0.0239 \sin \alpha - 0.000682T_a + 0.0195\phi \quad (7)$$

For $0.3 < k_t < 0.78$

$$\frac{I_d}{I} = 1.329 - 1.716k_t + 0.267 \sin \alpha - 0.00357T_a + 0.106\phi \quad (8)$$

For $k_t \geq 0.78$ & $\frac{I_d}{I} \geq 0.1$

$$\frac{I_d}{I} = 0.426k_t - 0.256 \sin \alpha + 0.00349T_a + 0.0734\phi \quad (9)$$

Where, I_d is diffuse horizontal irradiance, I is global horizontal irradiance, T_a is outdoor temperature and ϕ is relative humidity. For the locations, where temperature and relative humidity are not available:

For $k_t \leq 0.3$; $\frac{I_d}{I} \leq 1.0$

Models description

$$\frac{I_d}{I} = 1.02 - 0.254k_t + 0.0123 \sin \alpha \quad (10)$$

For $0.3 < k_t < 0.78$

$$\frac{I_d}{I} = 1.4 - 1.749k_t + 0.177 \sin \alpha \quad (11)$$

For $k_t \geq 0.78$ & $\frac{I_d}{I} \geq 0.1$

$$\frac{I_d}{I} = 0.486k_t - 0.182 \sin \alpha \quad (12)$$

The results showed that use of four variable correlation reduced residual sum of squares by 14.4 % when compared to a k_t correlation, derived from the same data. In current thesis, RBDH with four variable inputs was used in order to generate diffuse component of solar irradiance for the comparison with the other models.

3.1.1.3 Skartveith and Olseth

Olseth and Hollands 1987 developed a model for generation of diffuse fraction, using hourly data. k_t and solar altitude was used at a model mentioned above, which improved a model from 1998 by adding new parameters of hour to hour variability index and regional surface albedo as input data. Data sets from Bergen, Norway were used with data only for April to October due to a significant snow cover in other months of the year. For this study a snow-free case of SKOH has been considered for the comparison purpose.

3.1.1.3.1 *The variability index*

Clouds can affect diffuse and beam irradiance in various ways. For instance, dark clouds can have less diffuse in comparison to lighter ones. Moreover, height and thickness of the clouds can change the diffuse irradiation. A diagnostic tool to present the cloud conditions, which has a similar manner as Perez (1991), an hourly variability index σ_3 was introduced. It is defined as a root mean square of deviation between clear sky index of the time step (ρ_t) and, respectively, the preceding (ρ_{t-1}) and the subsequent (ρ_{t+1}) hour:

Models description

$$\sigma_3 = \sqrt{\frac{(\rho_t - \rho_{t-1})^2 + (\rho_t - \rho_{t+1})^2}{2}} \quad (13)$$

In the case, when the preceding or subsequent hour is missing, the following formula is used:

$$\sigma_3 = |\rho_t - \rho_{t\pm 1}| \quad (14)$$

Clear sky index ρ is:

$$\rho = \frac{k_t}{k_1} \quad (15)$$

And k_1 is:

$$k_1 = 0.83 - 0.56e^{-0.06 \times \alpha} \quad (16)$$

Where α is solar altitude in degrees.

σ_3 is almost independent of solar altitude. Low σ_3 shows overcast sky, which $0.9 < \rho_t < 1.0$ represents nearly cloudless sky. It was indicated that k_t for clear sky is only related to solar elevation and rarely reaches up to 0.75; higher k_t occurs in the case of dealing with partially cloudy sky with unobstructed sun disk in snow-free areas or locations with high surface albedo. In those cases, only diffuse component will increase, while amount of radiation coming directly from the sun remains constant. In appendix II, observation of various sky types and correlation of k_t with solar components is discussed.

If for any reason σ_3 is unknown, the following equation may be applied:

For $\rho < 1.04$:

$$\sigma_3 = 0.021 + 0.397\rho - 0.231\rho^2 - 0.13 e^{-\left\{\left[\frac{(\rho-0.931)}{0.134}\right]^2\right\}^{0.8334}} \quad (17)$$

For $\rho > 1.04$:

Models description

$$\sigma_3 = 0.12 + 0.65(\rho - 1.04) \quad (18)$$

3.1.1.3.2 Invariable hours

For $\sigma_3 = 0$, the diffuse fraction model is developed applying linear least square regression to Bergen's data for each bins (I-IV) of clearness index k_t , is as follow:

- i. For $k_t < 0.22$, SKOH considers a totally overcast sky without any direct beam irradiance:

$$k_d = 1.00 \quad (19)$$

- ii. For $0.22 \leq k_t \leq k_2$, Broken clouds and semi unobstructed sun dominates.

$$k_d = f(k_t, \alpha) = 1 - (1 - k_{d1})(0.11\sqrt{K} + 0.15K + 0.74K^2) \quad (20)$$

Where

$$K = 0.5(1 + \sin \left[\frac{k_t - 0.22}{k_1 - 0.22} \pi - 0.5\pi \right]) \quad (21)$$

$$k_2 = 0.95k_1 \quad (22)$$

$$k_{d1} = 0.07 + 0.046 \frac{90 - \alpha}{\alpha + 3} \quad (23)$$

For α less than 1.4° k_{d1} considered as 1.

- iii. For $k_2 \leq k_t \leq k_{max}$, an almost cloudless sky was assumed. Thus, diffuse component will be constant, and diffuse fraction will be dependent on solar elevation and turbidity. From this assumption:

$$k_d = k_{d2} k_2 \frac{(1 - k_t)}{k_t(1 - k_2)} \quad (24)$$

The upper limit k_{max} is derived from k_{bmax} :

Models description

$$k_{max} = \frac{k_{bmax} + \frac{k_{d2}k_2}{(1-k_2)}}{1 + \frac{k_{d2}k_2}{(1-k_2)}} \quad (25)$$

Where k_{bmax} is fitted to an extreme beam transmittance modelled by the SMARTS2 (Gueymard 1993):

$$k_{bmax} = 0.81^\omega \quad (26)$$

$$\omega = \frac{1^{0.6}}{\sin \alpha} \quad (27)$$

- iv. For $k_t \geq k_{max}$, they assumed that diffuse fraction is only influenced by clouds, due to the constant beam irradiance:

$$k_d = 1 - k_{max} \frac{1 - k_{dmax}}{k_t} \quad (28)$$

Where maximum diffuse fraction for maximum clearness index is:

$$k_{dmax} = k_{d2}k_2 \frac{(1 - k_{max})}{k_{max}(1 - k_2)} \quad (29)$$

3.1.1.3.3 Variable hours

For $\sigma_3 > 0$, the least square analysis indicated use of a term $\Delta(k_t, \alpha, \sigma_3)$, which should be added to the above invariable hours diffuse fraction for all bins (I to IV):

For $0.14 \leq k_t \leq k_x$:

$$\Delta(k_t, \alpha, \sigma_3) = -2k_L^2(1 - k_L)\sigma_3^{1.3} \quad (30)$$

For $k_x \leq k_t \leq k_x + 0.71$:

$$\Delta(k_t, \alpha, \sigma_3) = 3k_R(1 - k_R)^2\sigma_3^{0.6} \quad (31)$$

For $k_t > k_x + 0.71$ and for $k_t < 0.14$:

Models description

$$\Delta(k_t, \alpha, \sigma_3) = 0 \quad (32)$$

Where

$$k_x = 0.56 - 0.32e^{-0.06\alpha} \quad (33)$$

$$k_L = \frac{k_t - 0.14}{k_x - 0.14} \quad (34)$$

$$k_R = \frac{k_t - k_x}{0.71} \quad (35)$$

3.1.2 Logistic function models

3.1.2.1 Boland

Boland et al. 2001, made an attempt on finding a model for the whole range of k_t , unlike previous models such as Erbs et al. 1982, Reindl et al. 1990, Olseth and Hollands 1987, and Spencer 1982, which split data according to different ranges of k_t . Accordingly, he used logistic function that could fit the data. Using curve fitting tool he derived two equations, (3.18) for 15 minutes data and (3.19) for hourly data:

$$\frac{I_d}{I} = \frac{1}{1 + e^{8.645(k_t - 0.613)}} \quad (36)$$

$$\frac{I_d}{I} = \frac{1}{1 + e^{7.997(k_t - 0.586)}} \quad (37)$$

Mentioned model was compared with Reindl model and showed slight improvement in the statistical measures such as R-square and Composite Residual sum of squares (CRSS). The main advantage of Boland model is the use of one single equation for the whole range of k_t . This equation predicts low diffuse fraction for high k_t , which is not the case in reality and due to the sky with visible

Models description

sun and partly cloudy, k_t will reach near 0.9. Consequently, there will be high diffuse irradiance as a result of reflection of clouds.

3.1.2.2 Boland-Ridley-Lauret (BRL)

Employing a Bayesian framework, Lauret et al. 2010 derived a simple logistic hourly model by using 5 variables, which are apparent solar time (AST), solar altitude α , clearness index k_t , daily clearness index K_t and persistence index ψ . Application of these variables enhances the performance of the predictive model due to their characteristics. The proposed model is:

$$\frac{I_d}{I} = \frac{1}{1 + e^{-5.32+7.28k_t-0.03AST-0.0047\alpha+1.72K_t+1.08\psi}} \quad (38)$$

$$K_t = \frac{\sum_{i=1}^{24} I_i}{\sum_{i=1}^{24} I_{0,i}} \quad (39)$$

$$\psi = \begin{cases} \frac{k_{t+1} + k_{t-1}}{2} & \text{sunrise } < t < \text{ sunset} \\ k_{t+1} & \\ k_{t-1} & \text{t=sunrise} \end{cases} \quad (40)$$

3.1.3 Exponential Models

Maxwell 1987 introduced an exponential model based on physical principles by developing a computer program, called the Direct Insolation Simulation Code (DISC model). Following this step, Perez (1991) used Maxwell beam irradiance for his first model, applying correcting coefficients to predict beam irradiance more accurately. His second model is air-mass independent.

3.1.3.1 Maxwell

Maxwell 1987 predicted normal beam irradiation I_b from hourly global irradiation values, using quasi-physical model. The amount of diffuse fraction can be calculated in order to compare it with other models. Initially, Maxwell calculated a maximum k_t for clear sky $K_{n,c}$:

Models description

$$K_{n,c} = 0.866 - 0.122m_{air} + 0.0121m_{air}^2 - 0.000653m_{air}^3 + 0.000014m_{air}^4 \quad (41)$$

In which m_{air} is air mass depending on solar altitude (\emptyset):

$$m_{air} = \frac{1}{\sin(\emptyset) + \frac{0.50572}{(\emptyset + 6.07995)^{1.6364}}} \quad (42)$$

Then a reduction ΔK_n of the maximum is considered:

$$\Delta K_n = a + be^{cm_{air}} \quad (43)$$

Where parameters of a, b and c are determined for two ranges of k_t , using two equations below:

$$\text{If } k_t \leq 0.6 \quad \begin{cases} a = 0.512 - 1.560k_t + 2.286k_t^2 - 2.222k_t^3 \\ b = 0.370 + 0.962k_t \\ c = -0.280 + 0.932k_t - 2.048k_t^2 \end{cases} \quad (44)$$

$$\text{If } k_t > 0.6 \quad \begin{cases} a = -5.743 + 21.77k_t - 27.49k_t^2 + 11.56k_t^3 \\ b = 41.4 - 118.5k_t + 66.05k_t^2 + 31.9k_t^3 \\ c = -47.01 + 184.2k_t - 222k_t^2 + 73.81k_t^3 \end{cases} \quad (45)$$

Finally, the direct normal irradiance and diffuse horizontal irradiance can be derived using:

$$I_{b,Disk} = I_0 \cdot K_n \quad (46)$$

$$I_d = I - I_{b,Disk} \sin \alpha \quad (47)$$

3.1.3.2 Perez

Perez et al. 1991 used a statistical approach from a large multi-climatic experimental database to derive two models for converting hourly global irradiance into hourly direct beam irradiance. This approach was based on the parameterization of insolation conditions (Perez et al. 1990), using four

Models description

dimensional space. In the current thesis the first model was used. Direct normal beam irradiance is:

$$I = I_{b,disk} \cdot X(K'_t, Z, W, \Delta K'_t) \quad (48)$$

Where I_{disk} the direct normal irradiance is estimated by the DISC model (Maxwell 1987) and $X(K'_t, Z, W, \Delta K'_t)$ is a coefficient made of four insolation condition parameters, which are adjusted clearness index (K'_t) that represents meteorologically similar conditions irrespective of the position of the sun (equation 49). Z is the solar zenith angle (equation 50), $\Delta K'_t$ stability index (equation 51) and W is atmospheric precipitable water (equation 52). These coefficients are obtained from a look-up table consisting of a $6 \times 6 \times 5 \times 7$ matrix (See Table 3-2). As for the second model, he used two terms of a and b, which were derived statistically from a large multi-climatic experimental data set. These coefficients are the average of 500 data points and were obtained from a four dimensional look-up table consisting of $8 \times 5 \times 4 \times 6$ matrixes (Table 3-3).

$$K'_t = \frac{k'_t}{1.031 \left(e^{\left(\frac{-1.4}{0.9 + \frac{9.4}{m_{air}}} \right)} + 1 \right)} \quad (49)$$

$$Z = 90 - \alpha \quad (50)$$

$$\Delta K'_t = 0.5 (|K'_t - K'_{t+1}| + |K'_t - K'_{t-1}|) \quad (51)$$

$$W = e^{(0.07T_d - 0.075)} \quad (52)$$

Models description

Table 3-2. Bins used in Perez function

Bins	K'_t	Z (°)	W (cm)	$\Delta K'_t$
1	0.00-0.24	00-25	0-1	0.000-0.015
2	0.24-0.40	25-40	1-2	0.015-0.035
3	0.40-0.56	40-55	2-3	0.035-0.070
4	0.56-0.70	55-70	3-∞	0.070-0.150
5	0.70-0.80	70-80	0-∞	0.150-0.300
6	0.80-1.00	80-90		0.399-1.000
7				0.000-1.000

Table 3-3. Bins used for the Perez second model

Bins	K'_t	Z (°)	W (cm)	$\Delta K'_t$
1	0.00-0.29	0.0-40.0	0-1.50	0.000-0.020
2	0.29-0.42	40.0-52.5	1.50-2.75	0.020-0.048
3	0.42-0.53	52.5-65.0	2.75-∞	0.048-0.110
4	0.53-0.64	65.0-75.0	0.00-∞	0.110-0.250
5	0.64-0.71	75.0-90.0		0.250-1.000
6	0.71-0.75			0.000-1.000
7	0.75-0.79			
8	0.79-1.00			

3.1.4 Development of a new hourly Model for Vienna

Previous studies by Dervishi and Mahdavi 2012 and Vazifeh et al. 2013 concluded vulnerability of the existing models for prediction of solar component (diffuse and direct beam insolation) for location of Vienna, Austria. In appendix II, different sky conditions and their correlation with the clearness index has been discussed, using a physical approach. This approach can be used for generating a global model. Though, in order to have a simple local model, curve fitting has been considered for model generation.

In this work, a new model has been developed, based on measurement data of Vienna, using piecewise function. Five ranges of clearness index have been chosen for its development. The function for each range of clearness index is derived using linear least square regression. 6 variables were used to derive a model, namely clearness index k_t , daily clearness index K_t (Equation 54), solar altitude α , temperature T_a , precipitable water W , and apparent solar time (AST). AST is symmetric around solar noon and shows the

Models description

difference between morning and afternoon. A list of variable predictors and they format being used for the model is demonstrated in *Table 3-4*. These predictors have been selected by looking at the correlation with the clearness index by fixing the other parameters, although having a low correlation. General formulation has been used is ψ^m , in which ψ is a transformed format of variables in range of 0 to 1 (See *Table 3-4*), and m is derived based on the minimum of the *RMSE* of the result and maximum of the R^2 as well. The general formation of diffuse fraction is:

$$a_0 + a_1\psi_1^{m_1} + a_2\psi_2^{m_2} + a_3\psi_3^{m_3} + a_4\psi_4^{m_4} + a_5\psi_5^{m_5} + a_6\psi_6^{m_6} \quad (53)$$

$$K_t = \frac{\sum_1^{24} k_t}{24} \quad (54)$$

- First variable is in the formulation of $(1 - 0.1W)^{0.01 \times n}$, in which n is the number of iterations. Using a loop in the Matlab environment n varied from 1 to 1000 to find the best fitting for the precipitable water (See *Figure 3-1*) and is equal to 8.34. Then the correlation is:

$$(1 - 0.1W)^{8.34}$$

Table 3-4. Variables used in Vienna model

Variables	Symbols	formulation
Clearness Index	k_t	$(1 - 0.1W)^{8.34}$
Solar altitude	α	$(\frac{\alpha}{90})^{0.78}$
Temperature	T	$(1 - k_t)^{1.73}$
Precipitable water	W	$(1 - K_t)^{1.38}$
Apparent solar time	AST	$(1 - \frac{(T + 20)}{70})^{0.58}$
Daily clearness index	K_t	$(\frac{ AST }{8})^{9.84}$

Models description

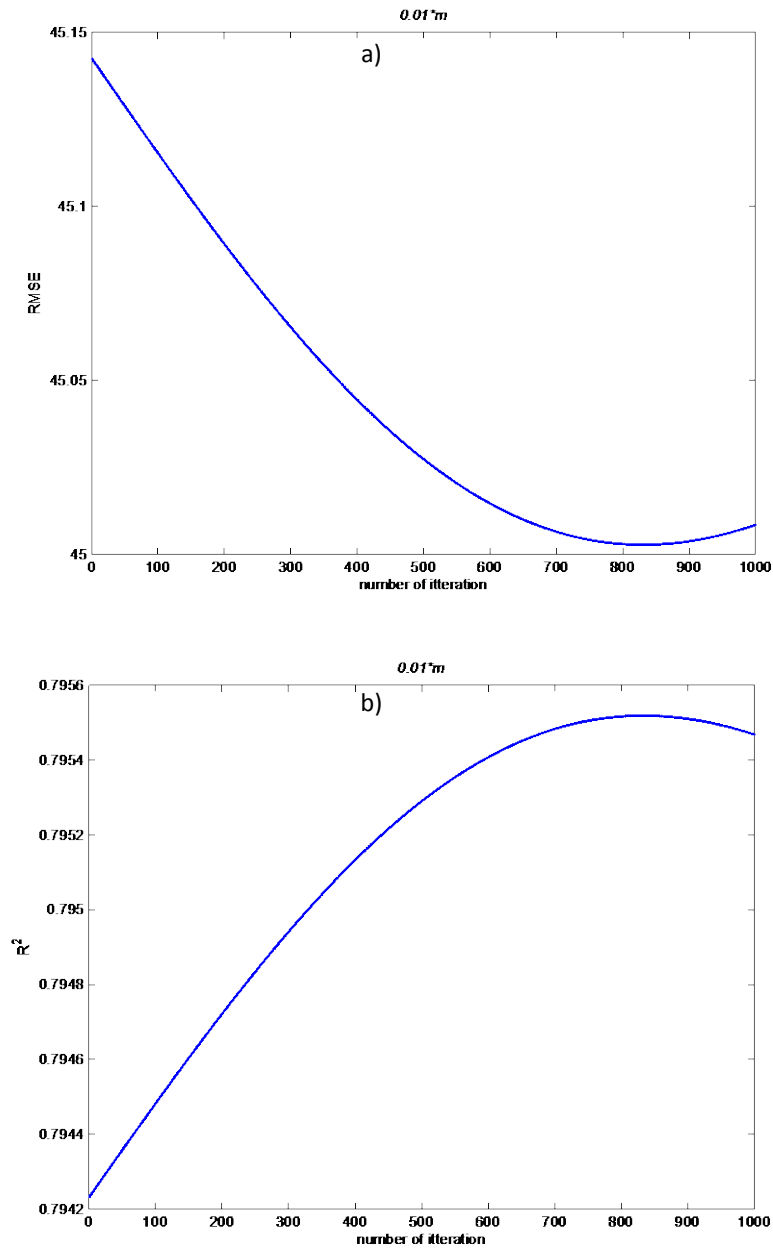


Figure 3-1. a) RMSE for predicted diffuse horizontal irradiance for each iteration b) R² for predicted diffuse horizontal irradiance for each iteration

- Second variable is in the format of $(\frac{\alpha}{90})^{0.01 \times n}$ in which n is the number of iteration (See Figure 3-2) and is equal to 0.78. Then the correlation is:

$$\left(\frac{\alpha}{90}\right)^{0.78}$$

Models description

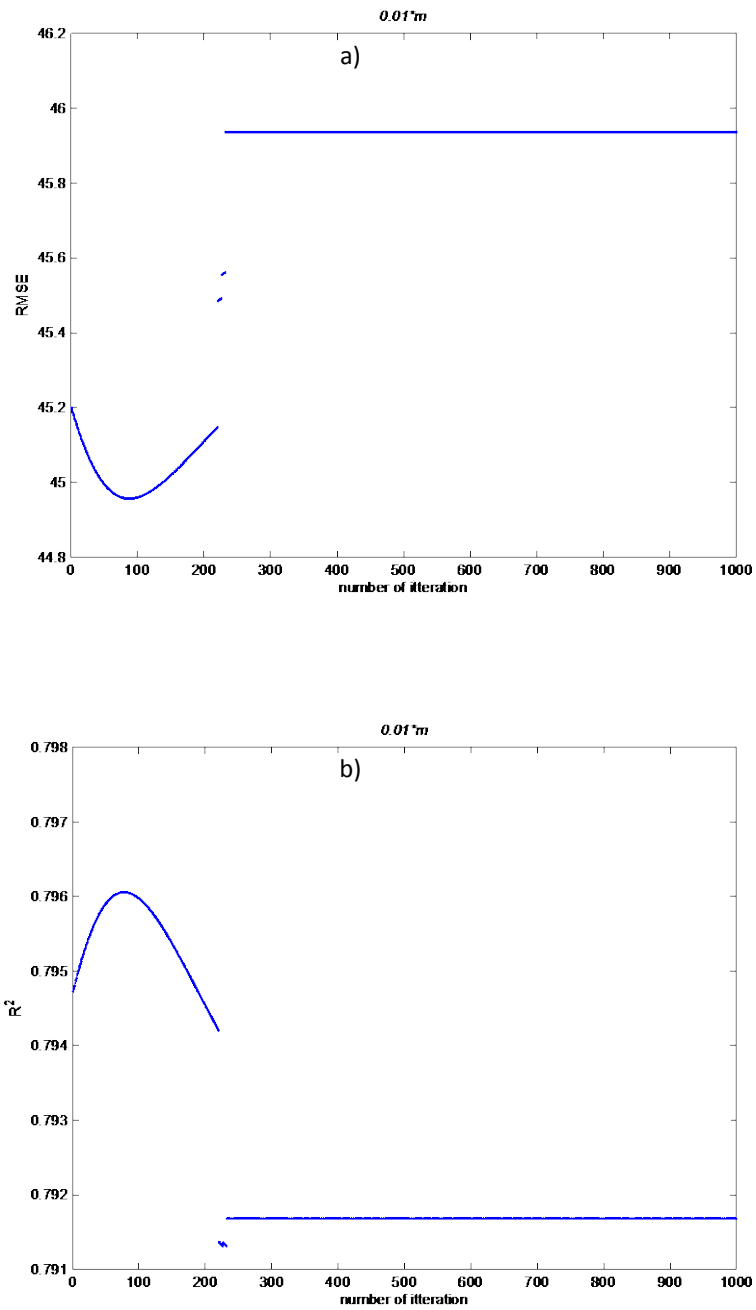


Figure 3-2. a) RMSE for predicted diffuse horizontal irradiance for each iteration b) R^2 for predicted diffuse horizontal irradiance for each iteration

Models description

- Third variable is in the format of $(1 - k_t)^{0.01 \times n}$ in which n is the number of iteration (See *Figure 3-3*) and is equal to 1.73. Then the correlation is:

$$(1 - k_t)^{1.73}$$

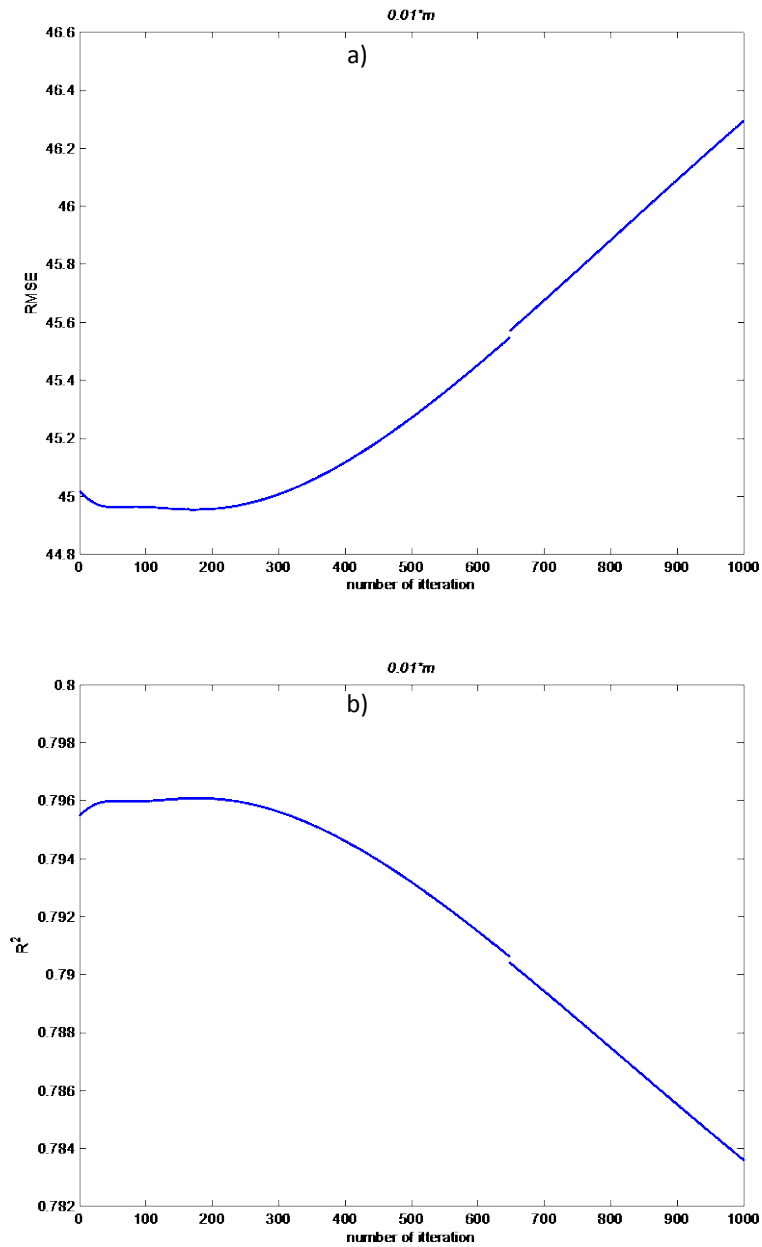


Figure 3-3. a) RMSE for predicted diffuse horizontal irradiance for each iteration b) R² for predicted diffuse horizontal irradiance for each iteration

Models description

- Forth variable is in the format of $(1 - K_t)^{0.01 \times n}$ in which n is the number of iteration (See *Figure 3-4*) and is equal to 1.38. Then the correlation is:

$$(1 - K_t)^{1.38}$$

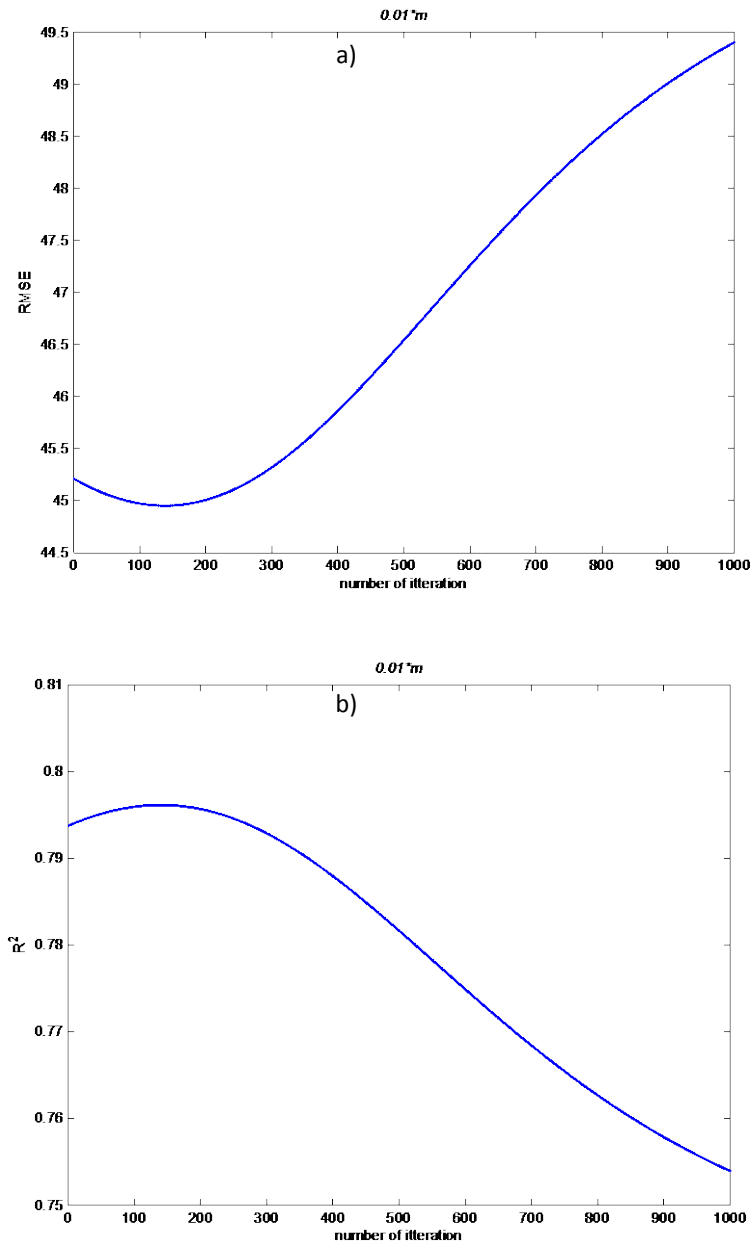


Figure 3-4. a) RMSE for predicted diffuse horizontal irradiance for each iteration b) R2 for predicted diffuse horizontal irradiance for each iteration

Models description

- Fifth variable is in the format of $(1 - \frac{(T+20)}{70})^{0.01 \times n}$ in which n is the number of iteration (See *Figure 3-5*) and is equal to 0.58. Then the correlation is:

$$(1 - \frac{(T + 20)}{70})^{0.58}$$

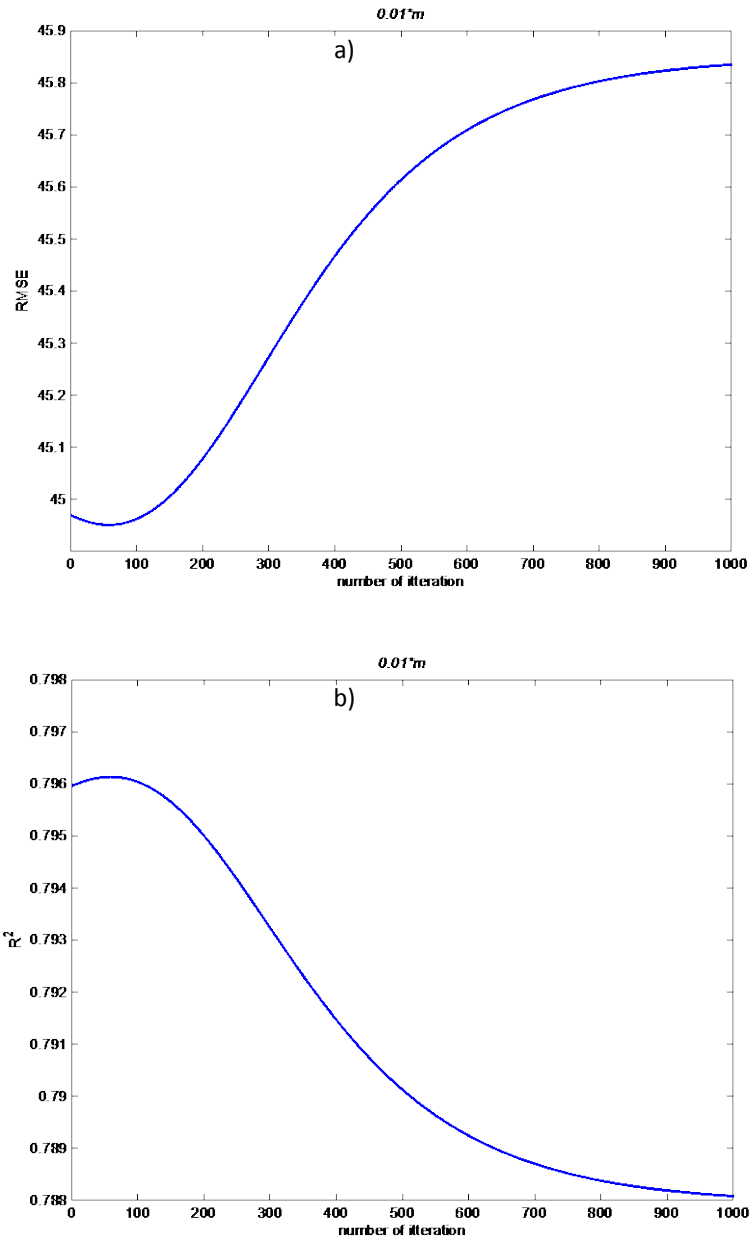


Figure 3-5. a) RMSE for predicted diffuse horizontal irradiance for each iteration b) R2 for predicted diffuse horizontal irradiance for each iteration

Models description

- Last variable is in the format of $\left(\frac{AST}{8}\right)^{5+0.01 \times n}$ in which n is the number of iteration (See *Figure 3-6*) and is equal to 9.84. Then the correlation is:

$$\left(\frac{AST}{8}\right)^{9.84}$$

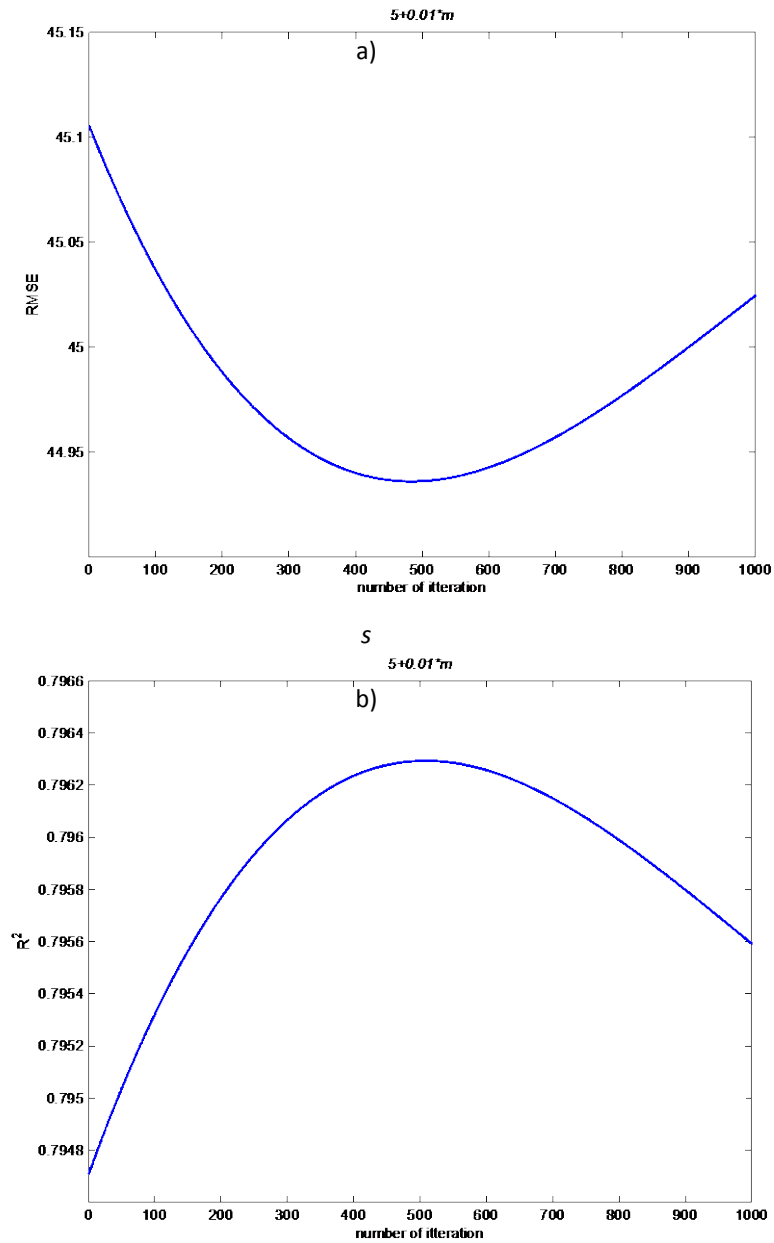


Figure 3-6. a) RMSE for predicted diffuse horizontal irradiance for each iteration b) R2 for predicted diffuse horizontal irradiance for each iteration

Models description

A linear least square regression method is used to adopt the model parameters for each range of clearness index (See *Table 3-5*) in Matlab modelling environment. The format of each function is as follow:

Table 3-5. parameters for the Vienna model

	$0 < k_t \leq 0.2$	$0.2 < k_t \leq 0.4$	$0.4 < k_t \leq 0.6$	$0.6 < k_t \leq 0.8$	$0.8 < k_t \leq 1.0$
$(1 - 0.1W)^{8.34}$	-0.0487	-0.4153	-0.1927	0.1253	-0.1002
$(\frac{\alpha}{90})^{0.78}$	0.8633	4.2370	5.1196	1.5092	-4.8227
$(1 - k_t)^{1.73}$	-0.1001	0.6667	1.6698	0.9327	-3.1605
$(1 - K_t)^{1.38}$	0.00045	0.1718	0.5543	0.8203	0.4480
$(1 - \frac{(T + 20)}{70})^{0.58}$	0.2286	1.0571	0.9206	0.1421	-0.2607
$(\frac{ AST }{8})^{9.84}$	0.0947	0.1875	0.6943	1.5818	0.0204
1	0.8861	-0.2189	-0.7741	-0.2356	0.5980

3.2 Radiance distribution model

Obtaining the distribution and magnitude of the light coming from the window, which correlates with the luminance distribution on the sky, is crucial. In this thesis, by using sky scanner data for 2011 (Weather station at Building Physics and Building Ecology department of Vienna University of technology, Vienna, Austria), a model was developed for prediction of the radiance and luminance distribution over the sky dome, using Skartveit (1998) clear sky definition. The models' performance worsens under all sky conditions due to the rise of complexity of clouds' nature, such as its distribution through the sky, thickness, shape and color.

Figure 3-7, demonstrates the correlation of angular distance between sky patch and sun position versus 'Radiance coefficient RC , as contribution of radiance of a patch to the sum of the Radiance of all 145 patches' in percent.

The correlation will significantly increase by applying it to the clear sky defined by Skartveit (1998). For this purpose, the variability index σ_3 of Skartveit (1998) and clear sky index ρ are calculated for each measurement. Data having $\sigma_3 = 0$ and $0.9 < \rho < 1.0$ are considered as clear sky (See *Figure 3-8*). In order to narrow down the deviation impact of patch altitude is considered by dividing the sky into a number of rings. This is done by dividing the patches according to different

Models description

patch altitudes. Figures on pages 28 to 30, demonstrate the correlation of angular distance between sun disk and sky patch for each sky ring.

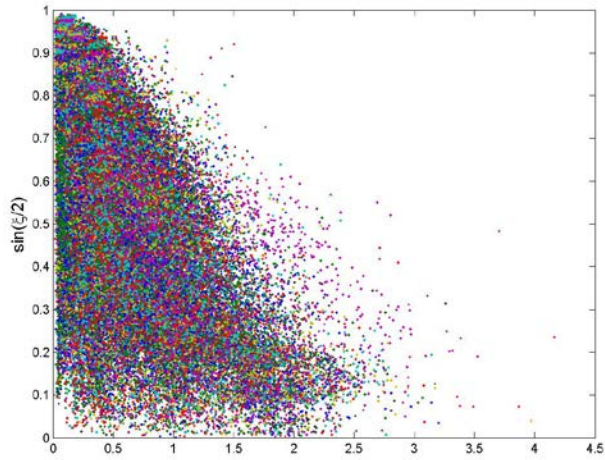


Figure 3-7. Correlation of Radiance Coefficient versus angular distance between sun disk and patch center under all weather conditions

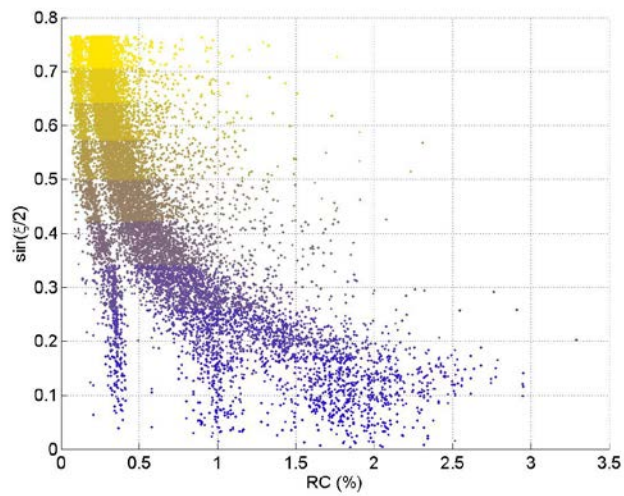


Figure 3-8. Correlation of Radiance Coefficient versus angular distance between sun disk and patch center (Clear days)

Models description

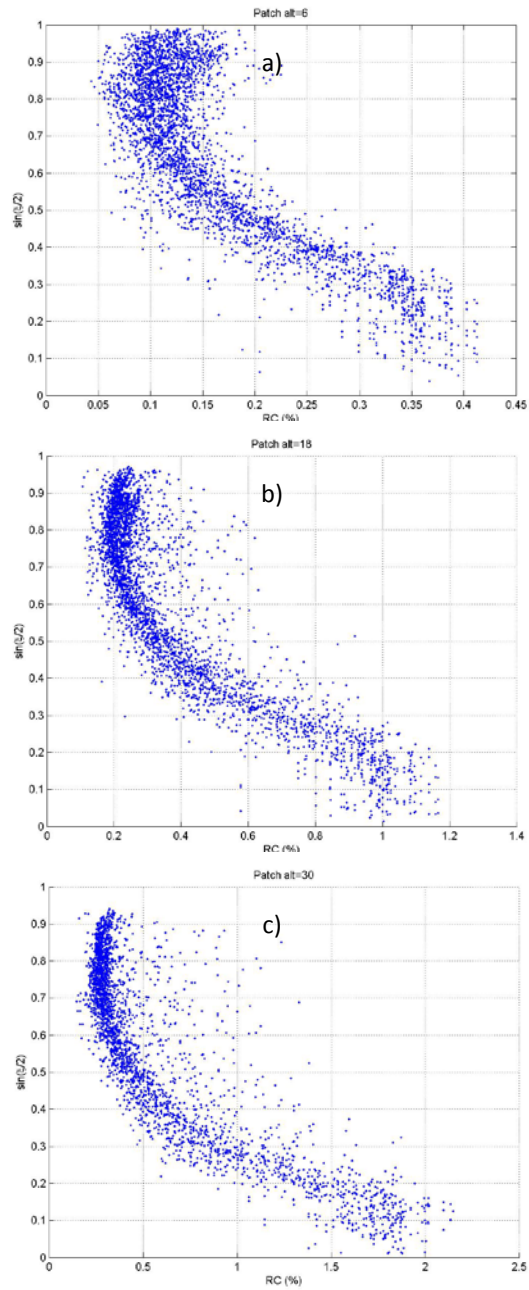


Figure 3-9. Radiance coefficients for each ring versus sinus of half angular distance between patch center and sun disk (a) Patch altitude = 6°, b) Patch altitude = 18°, and c) Patch altitude = 30°)

Models description

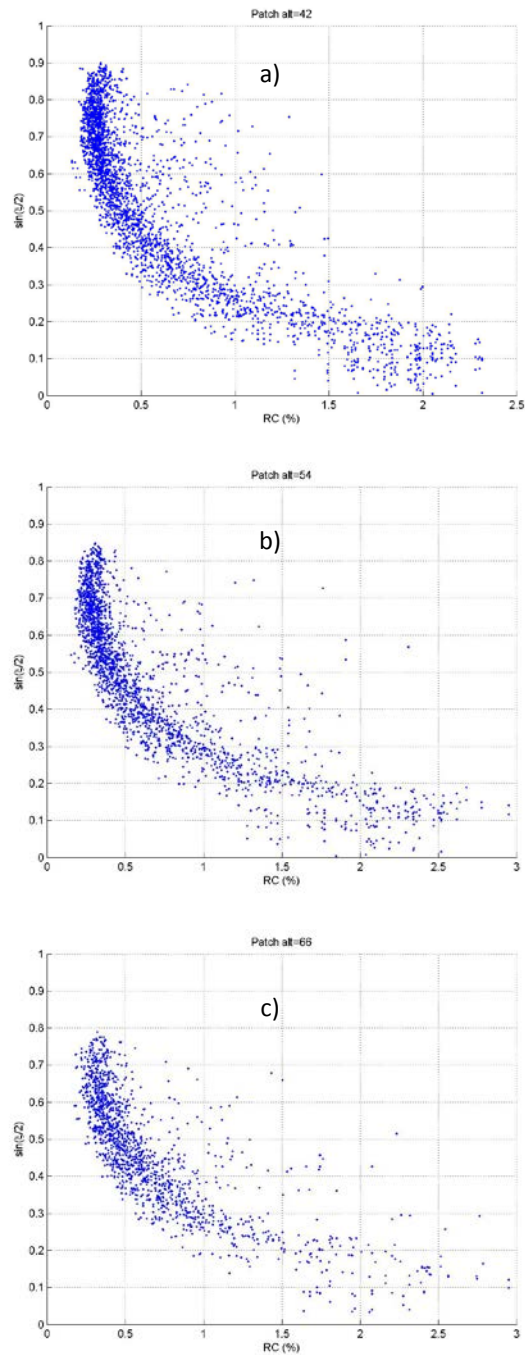


Figure 3-10. Radiance coefficients for each ring versus sinus of half angular distance between patch center and sun disk (a) Patch altitude = 42°, b) Patch altitude = 54°, and c) Patch altitude = 66°)

Models description

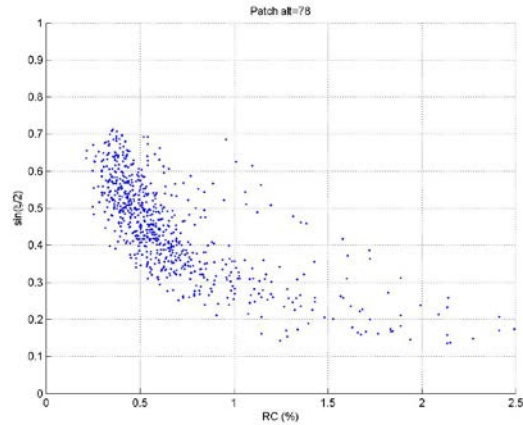


Figure 3-11. Radiance coefficients for each ring versus sinus of half angular distance between patch center and sun disk (Patch altitude = 78)

Curve fitting procedure has been used for each ring of sky patches to adopt the correlations (See pages 45 to 47). Four degrees polynomial function using $\sin(\frac{\xi}{2})$ (sinus of half of angular distance between sun disk and sky patch) as a variable has been applied. Coefficients for each sky ring are given in Table 3-6. A performance evaluation has been done in Chapter 4 (See on page 44).

Table 3-6. Parameters of RC model functions for clear sky

Patch altitude	$\sin(\frac{\xi}{2})^3$	$\sin(\frac{\xi}{2})^2$	$\sin(\frac{\xi}{2})$	1
6° RC (%)=	0.8645	-0.8618	-0.2776	0.4299
18° RC (%)=	0.77820	0.4545	-2.155	1.244
30° RC (%)=	-1.007	4.946	-5.793	2.288
42° RC (%)=	-2.541	7.647	-7.199	2.46
54° RC (%)=	-2.22	8.058	-8.066	2.768
66° RC (%)=	-3.014	9.626	-8.921	2.919
78° RC (%)=	-14.04	25.28	-15.62	3.745
87° RC (%)=	-24.44	40.89	-23.08	5.123

Chapter 4

Results & Discussions

4.1 Model performances

All models are implemented using Matlab environment. As discussed in Chapter 3, some of the models were identified for the location of Vienna. Predicted diffuse horizontal irradiance of each model is compared with the measured data from two above mentioned weather stations in Vienna city. Statistical measures applied for the comparison are discussed at part 4.2 in details. A short overview of the models implementation and evaluation process is given in this part (See *Figure 4-1*). *Figure 4-13*, illustrates the R-square of the models for 5 ranges of clearness index, which will be discussed for each model individually.

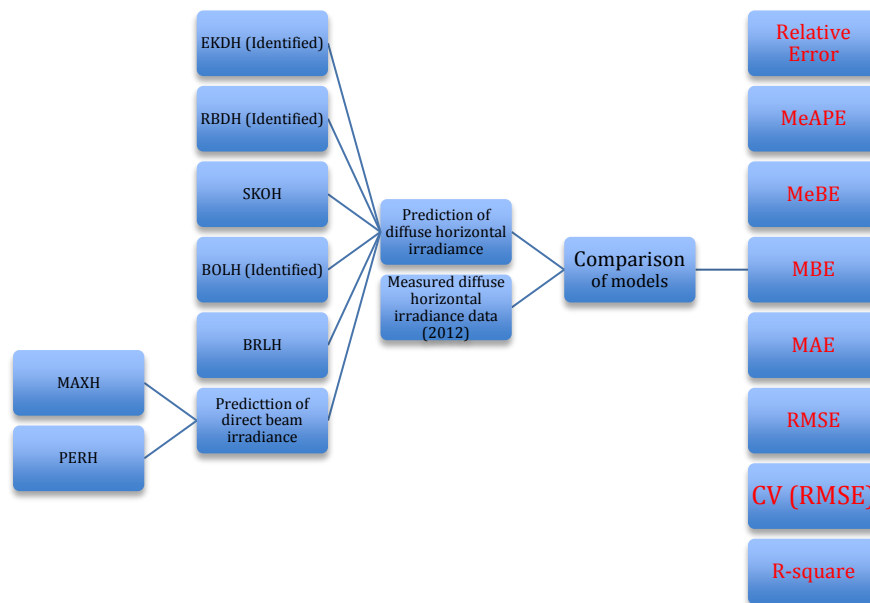


Figure 4-1. Schema for the models implementation and evaluation process

4.1.1 Erbs et al.

EKDH depends only on k_t as a variable. *Figure 4-2-a*, illustrates EKDH diffuse horizontal irradiance versus measured data. EKDH overestimates diffuse horizontal irradiance for low diffuse values. Besides, it underestimates diffuse

Results & Discussions

horizontal irradiance for high diffuse horizontal irradiance measurements. Diffuse fraction versus k_t is shown in

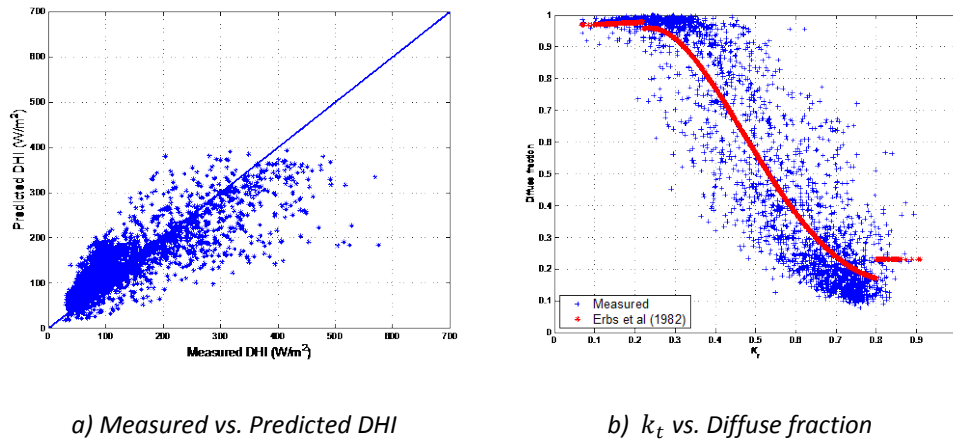


Figure 4-2. Comparison of Erbs et al. (1982) diffuse fraction model with measured data (year 2012)

Figure 4-2-b. Similar trend as Figure 4-2-a can be noticed for extreme low and high diffuse fractions. As it is shown, there is a huge range of diffuse fraction for each range of k_t , thus EKDH is not able to predict these values. Figure 4-13, shows that with increase of clearness index, EKDH R-square has a weakening trend down to around 0.3 for $0.8 < k_t < 1.0$. For that range of clearness index, EKDH only generates a constant diffuse fraction value, causing for that range EKDH R-square to stand in third place among the other models.

4.1.2 Reindl et al.

For work procedure with linear least square fitting, 4 parameters of RBDH were adapted for the location of Vienna, using 2011 BST weather station data. The coefficients are as follows:

For $k_t \leq 0.3$; $\frac{I_d}{I} \leq 1.0$

$$\frac{I_d}{I} = 0.9277 - 0.1667k_t + 0.0727 \sin \alpha - 0.0014T_a + 0.00075\phi \quad (55)$$

For $0.3 < k_t < 0.78$

$$\frac{I_d}{I} = 1.2775 - 1.626k_t + 0.1517 \sin \alpha - 0.0051T_a + 0.0023\phi \quad (56)$$

For $k_t \geq 0.78$; $\frac{I_d}{I} \geq 0.1$

Results & Discussions

$$\frac{I_d}{I} = 0.1156k_t - 0.169 \sin \alpha + 0.0048T_a + 0.0035\phi \quad (57)$$

Figure 4-3-a, demonstrates RBDH diffuse horizontal irradiance versus measured data. Similar to EKDH, RBDH overestimates diffuse horizontal irradiance for low diffuse values and underestimates it for high values of diffuse horizontal irradiance. Figure 4-3-b, diffuse fraction versus k_t is shown. Figure 4-13, shows that RBDH R-square similar to EKDH has a weakening trend with increase of clearness index but for $0.8 < k_t < 1.0$, this value increases and has the highest rate in comparison to the other models.

4.1.3 Skartveit and Olseth

As it is shown in Figure 4-4, SKOH can predict reasonable diffuse fraction values for high k_t , using variability index σ_3 and cloudless sky index ρ . the model performance decrease with increase of clearness index. (See Figure 4-12 and Figure 4-13).

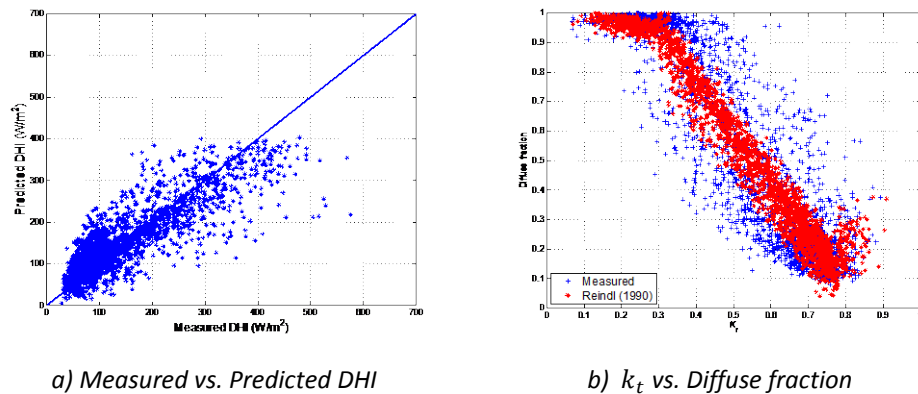


Figure 4-3. Comparison of Reindl (1987) diffuse fraction model with measured data (year 2012)

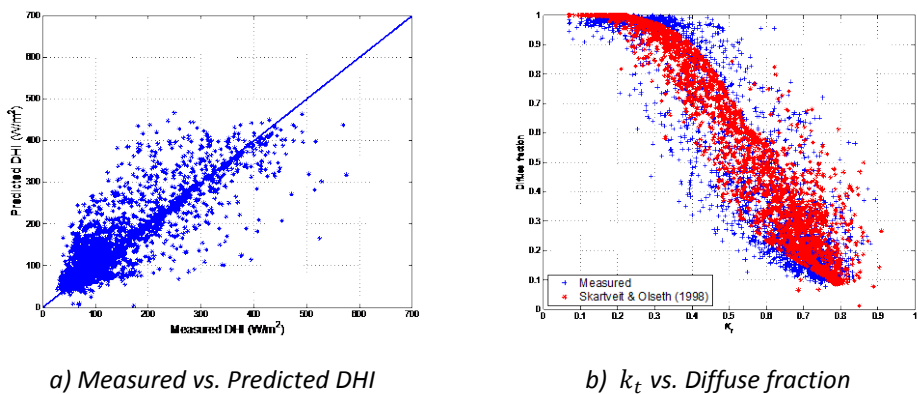


Figure 4-4. Comparison of Skartveit and Olseth (1998) diffuse fraction model with measured data (year 2012)

Results & Discussions

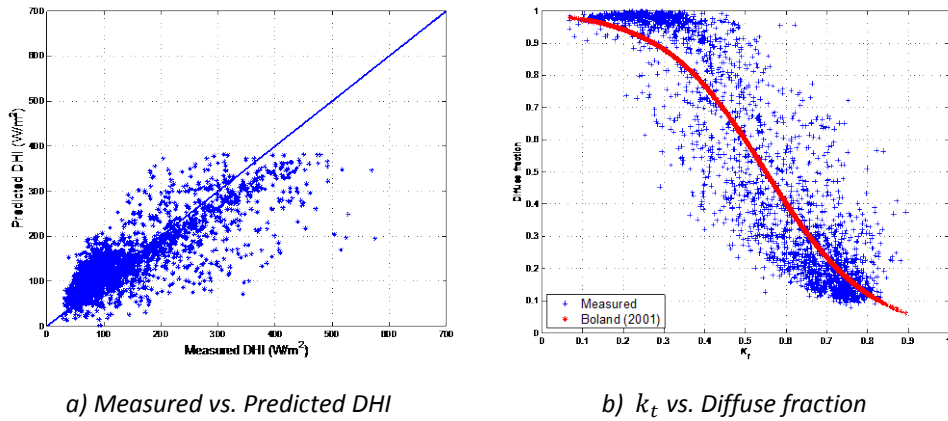


Figure 4-5. Comparison of Boland (2001) diffuse fraction model with measured data (year 2012)

4.1.4 Boland et al.

The BOLH was adapted for Vienna location, based on 2011 BST weather station data. The adapted version of BOLH is:

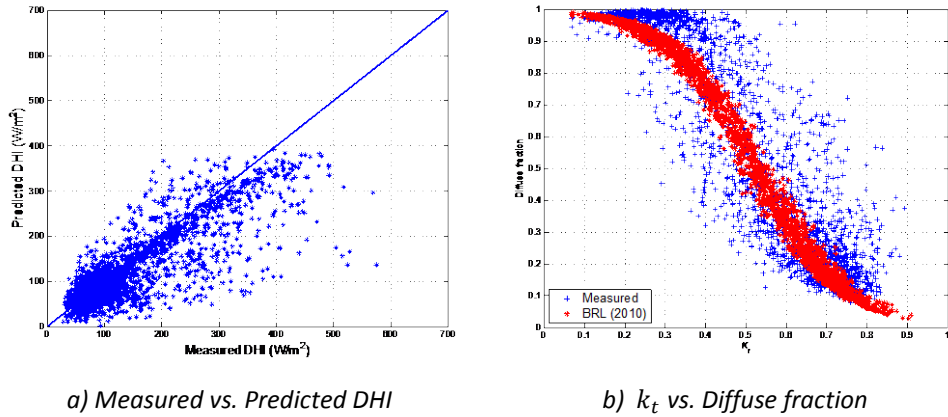
$$\frac{I_d}{I} = \frac{1}{1 + e^{7.9441k_t - 4.3663}} \quad (58)$$

Similar to EKDH, BOLH uses a single variable predictor of k_t . The only difference between the models is that BOLH uses logistic function for prediction of diffuse fraction, which is using only single function in order to predict diffuse fraction for whole range of k_t instead of using a piecewise polynomial function used in EKDH. The disadvantage of this function is that it underestimates the diffuse fraction for k_t higher than 0.8. (See Figure 4-5, Figure 4-12, and Figure 4-13)

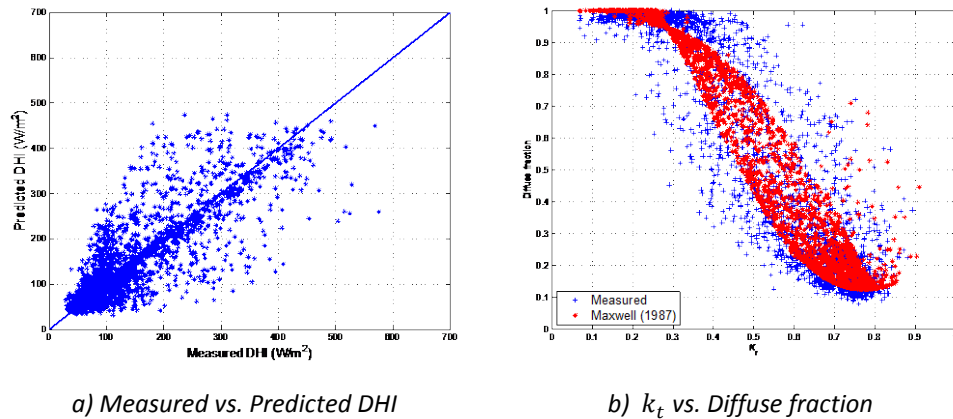
4.1.5 Boland-Ridley-Lauret

The BRLH is an enhanced model of the BOLH, introducing more variable predictors, but the same logistic function. Results are shown in Figure 4-6. An improvement in the prediction of diffuse fraction can be seen in comparison to the BOLH but with similar deficiency as the BOLH for k_t higher than 0.8.

Results & Discussions



a) Measured vs. Predicted DHI
b) k_t vs. Diffuse fraction
Figure 4-6. Comparison of BRL (2010) diffuse fraction model with measured data (year 2012)



a) Measured vs. Predicted DHI
b) k_t vs. Diffuse fraction
Figure 4-7. Comparison of Maxwell (1987) diffuse fraction model with measured data (year 2012)

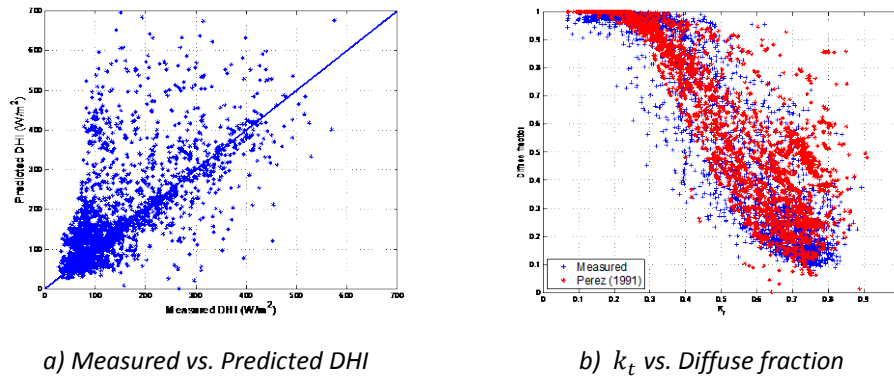
4.1.6 Maxwell

Clearness index versus diffuse fraction for measured data and data predicted by MAXH is demonstrated in *Figure 4-7*. It seems to perform better for low k_t , than for higher clearness index (See *Figure 4-12*, and *Figure 4-13*)

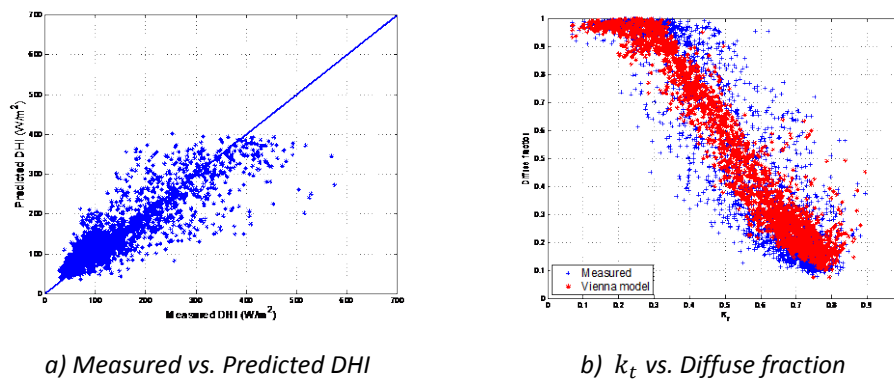
4.1.7 Perez

The PERH model has highest outliers among other models (See *Figure 4-8-a*), especially for higher clearness index (See *Figure 4-12*). The reason for such errors should be investigated and may be due to different approach for defining Perez model than the one done by the author of this thesis.

Results & Discussions



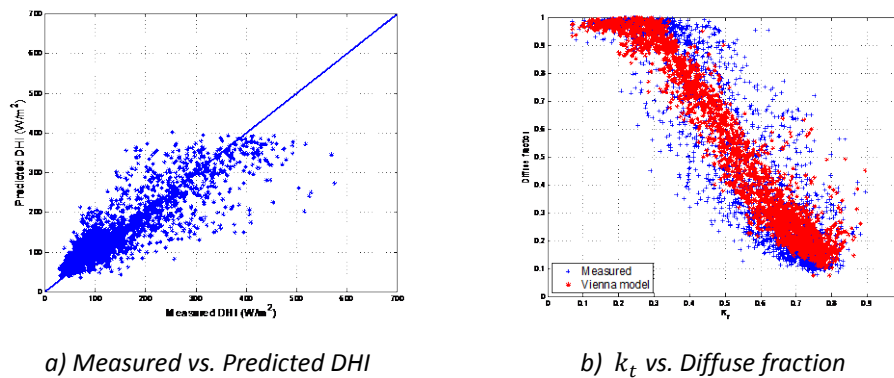
a) Measured vs. Predicted DHI
b) k_t vs. Diffuse fraction
Figure 4-8. Comparison of Perez (1991) diffuse fraction model with measured data (year 2012)



a) Measured vs. Predicted DHI
b) k_t vs. Diffuse fraction
Figure 4-9. Comparison of Vienna (2013) diffuse fraction model with measured data (year 2012)

4.1.8 New Model for Vienna

According to the statistical measures, Vienna model perform better than the other models. The performance decreases for higher clearness index similar to most of the models. For clear $0.8 < k_t < 1.0$, RBDH perform better than all other models, but the number of data with clearness index higher than 0.8 is slight (around 3% of total BPI data 2011).



a) Measured vs. Predicted DHI
b) k_t vs. Diffuse fraction
Figure 4-10. Comparison of Vienna (2013) diffuse fraction model with measured data (year 2012)

4.2 Models performance evaluation

For the evaluation of models performance, a number of statistical measures has been used, which are mostly considered by the models' authors, namely median of the absolute percentage error (MeAPE), median of bias error (MeBE), root mean square error (RMSE) which is a widely used statistical value, mean bias error (MBE), and mean absolute error (MAE). Moreover, CV (coefficient of variation of RMSE) for comparing the degree of variation between measured data and models. These measures' equations are:

$$MeAPE = median(|\frac{I_d - I_{msrd}}{I_{msrd}} \times 100|) \quad (59)$$

$$MeBE = median(\frac{I_d - I_{msrd}}{I_{msrd}}) \quad (60)$$

$$MBE = \frac{\sum_{i=1}^n (I_d - I_{msrd})}{n} \quad (61)$$

$$MAE = \frac{\sum_{i=1}^n (|I_d - I_{msrd}|)}{n} \quad (62)$$

$$RMSE = \sqrt{\frac{\sum_{i=1}^n (I_d - I_{msrd})^2}{n}} \quad (63)$$

$$CV = \frac{RMSE}{\bar{I}_{msrd}} \times 100 \quad (64)$$

Where I_d and I_{msrd} are model diffuse horizontal radiation and measured diffuse radiation respectively. The values of those statistical measures are given in Table 4-1, using two data sets of the BPI and the Hohe warte (2012). Superior performance of the Vienna model can be noted.

In addition, these values are plotted using bar graphs for BPI 2012 data set (See Figure 4-11). It can be noted that for both data sets the Vienna model has a better performance in all measures for both data sets except the Median of bias error. Moreover, a cumulative distribution function (CDF) of percentage of the results is used versus discrete values of Relative error RE (See Figure 4-14). This figure

Results & Discussions

demonstrates that for which percentages of the result we have at least certain Relative error. As it can be seen, the Vienna model includes more percentage of data for certain amount of Relative error among the other models. In addition to above mentioned statistical measures and to have a better understanding of models' performances, R-square for each range of clearness index has been calculated. Moreover, distribution of data for each range is plotted (See *Figure 4-13*).

Table 4-1. result of model comparison using mentioned statistical measures

Stations	Models	MBE(W/m ²)	MAE(W/m ²)	RMSE(W/m ²)	CV (RMSE) (%)	MeAPE	MeBE	R ²
BAUPHYSIC STATION 2012	EKDH	-0.74	42.59	60.00	37.06	19.28	0.0048	0.66
	RBDH	-1.52	38.29	54.07	33.40	16.99	0.0002	0.72
	SKOH	-10.19	41.30	60.70	37.49	17.33	-0.026	0.68
	BOLH	5.62	44.27	61.90	38.24	19.68	0.0423	0.64
	BRLH	28.80	46.44	69.57	42.98	18.77	0.096	0.62
	MAXH	-1.34	42.45	64.29	39.72	16.07	0.004	0.65
	PERH	-25.58	76.55	146.3	90.41	20.19	-0.036	0.24
	Vienna	-0.058	32.92	48.65	30.05	13.80	-0.009	0.77
HOHE WARTE STAT. 2012	EKDH	-3.97	34.36	51.11	37.78	14.92	0.022	0.70
	RBDH	-0.62	31.92	49.29	36.43	12.47	0.013	0.72
	SKOH	-10.70	33.38	52.55	38.85	13.30	0.0001	0.73
	BOLH	-3.25	36.33	52.62	38.89	16.83	0.05	0.69
	BRLH	19.61	34.11	52.69	38.95	14.73	0.042	0.72
	MAXH	-6.88	37.64	60.51	44.73	14.03	0.0012	0.66
	PERH	0.18	61.38	337.92	249.8	15.93	0.0004	0.06
	Vienna	-3.98	27.91	43.46	32.13	11.77	0.002	0.78

Results & Discussions

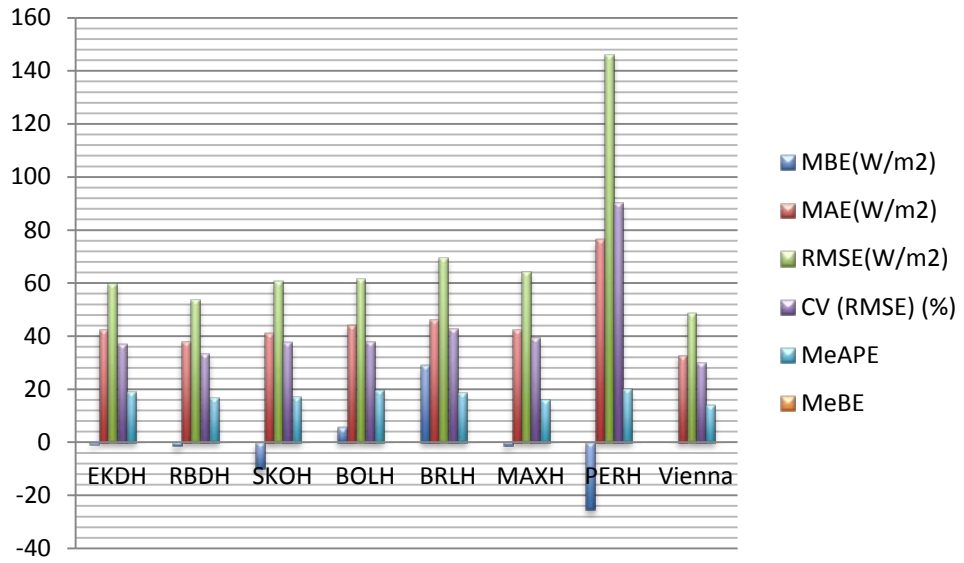


Figure 4-11. Bar graphs for statistical measures (BPI data set)

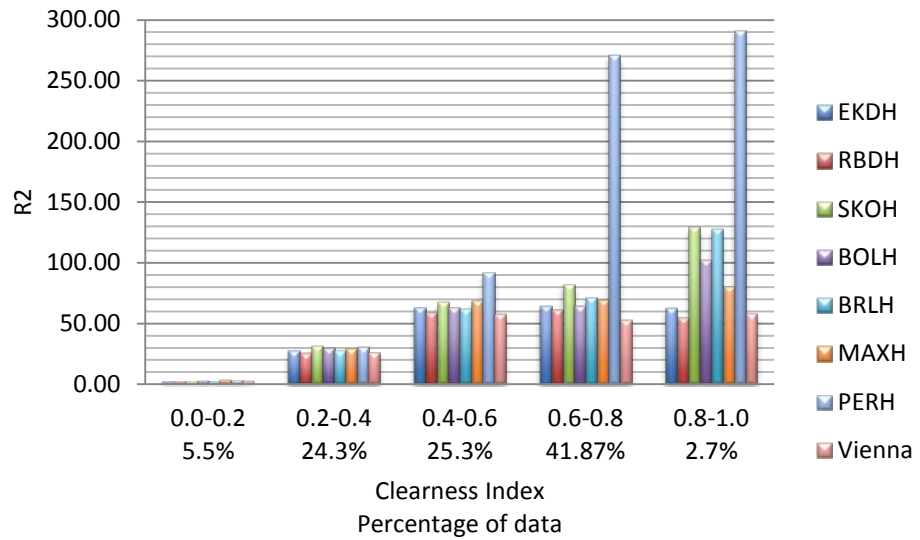


Figure 4-12. RMSE of models for each range of clearness Index and percentage of data for each range (BPI data 2011)

Results & Discussions

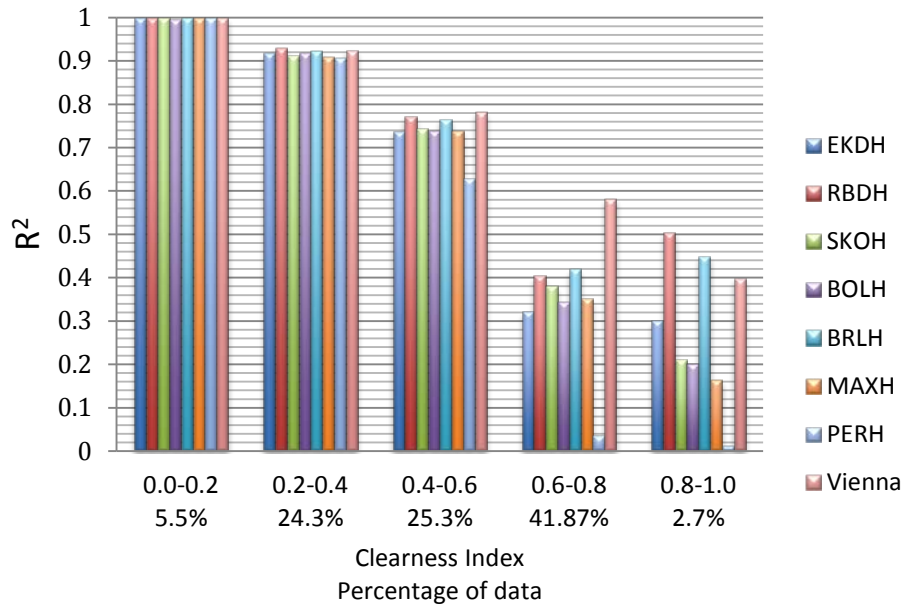


Figure 4-13. R-square of models for each range of clearness Index and percentage of data for each range (BPI data 2011)

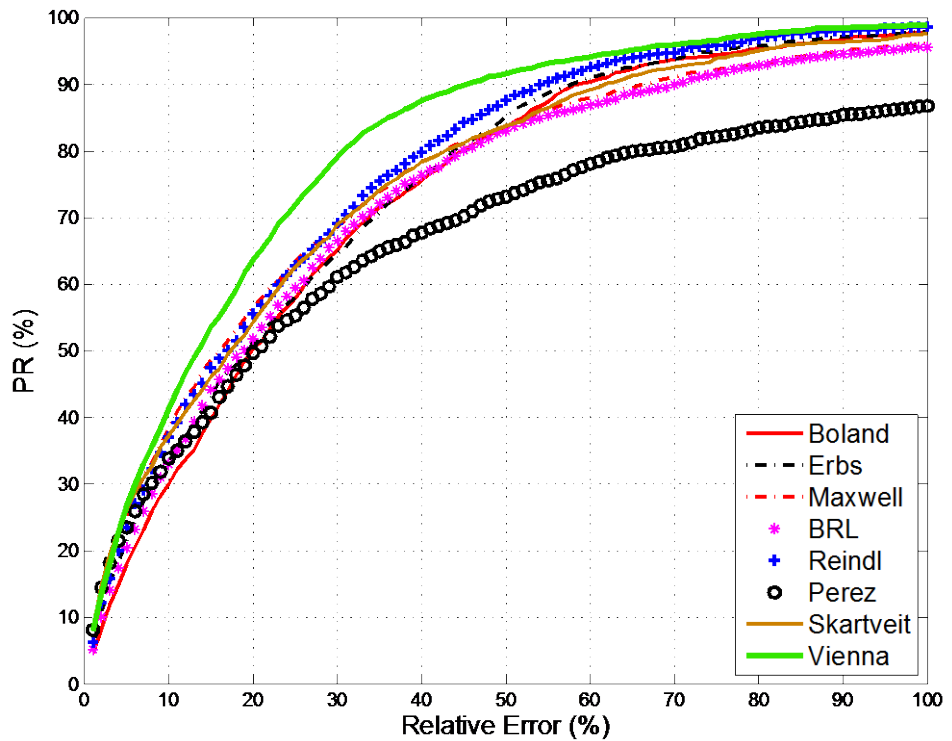


Figure 4-14. The cumulative distribution function (CDF) of the relative errors for all models (BPI data 2012)

4.3 Seasonal and solar impact

To have a better understanding of seasonal or solar impact, three procedure have been applied to the data: separation of seasons, separation of solar time (morning, midday, and afternoon) and different solar altitudes considered in the calculation of clearness index. Results are demonstrated in *Figure 4-15*, *Figure 4-16*, and *Figure 4-17*. With solar altitude increasing, a 4 o'clock direction shift can be noted in *Figure 4-15*, which indicates higher global radiation.

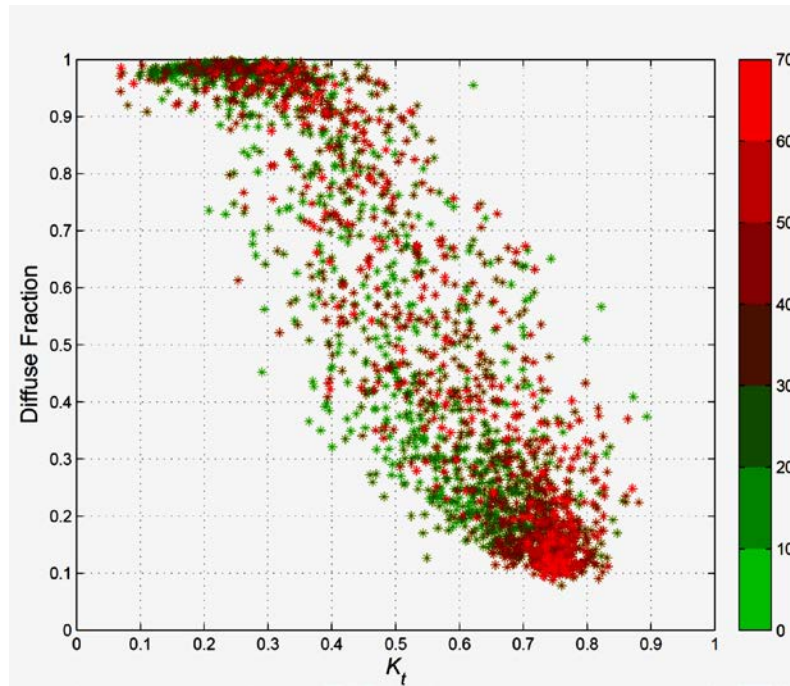


Figure 4-15. Impact of solar altitude on fraction of diffuse radiation (BPI data 2011)

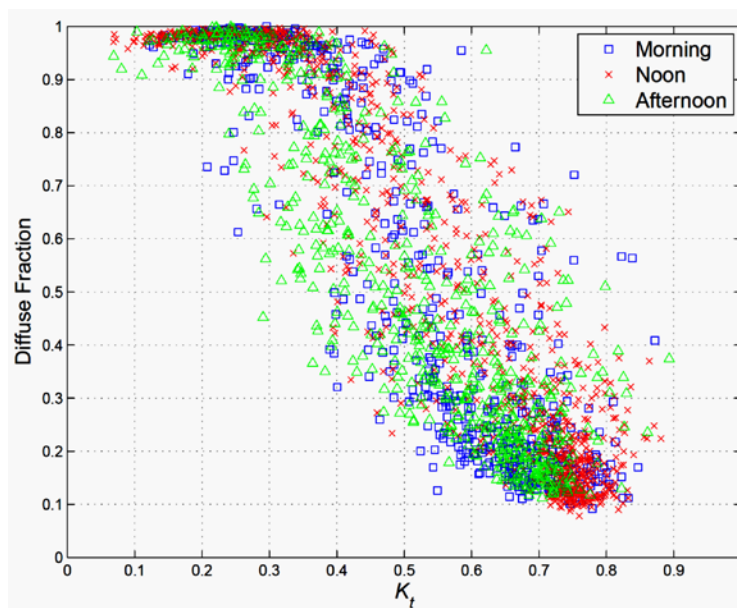


Figure 4-16. Impact of solar time on diffuse radiation (BPI data 2011)

Results & Discussions

Figure 4-16, has a similar trend with Figure 4-15, which can be explained by the fact that lower solar altitude can be expected in the morning and afternoon. A slight difference between these two figures can be explained due to the variation of solar altitude' range during the year.

Different seasons' impact on solar radiation may be expected due to the variation of:

- Different sun declination, which impacts global radiation directly
- Different average seasonal cloud cover
- Different average seasonal solar altitude
- Meteorological variables i.e. air temperature, relative humidity etc.

However, no significant difference due to different season can be seen in Figure 4-17.

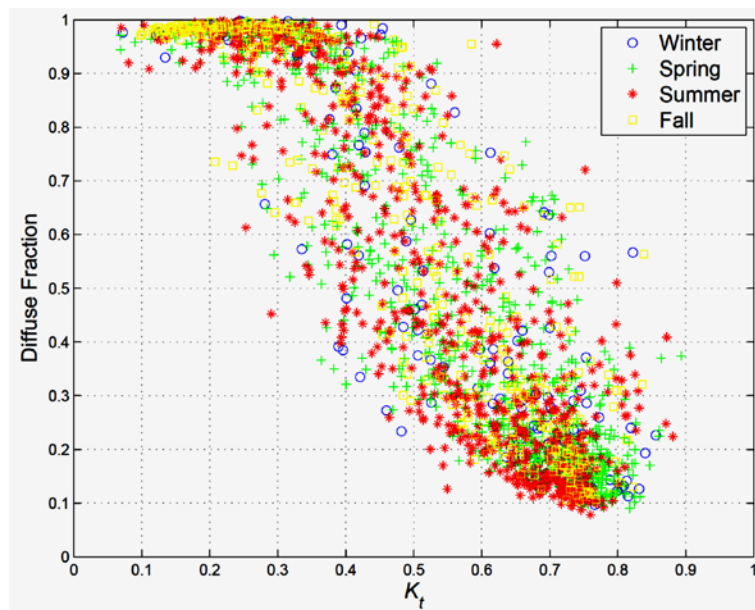


Figure 4-17. Season impact on diffuse radiation (BPI data 2011)

4.4 Diffuse model verification

For verification of developed model, measurement data collected during the year 2011 has been applied. Similar statistical measures were used in order of comparison (See Table 4-2). Results indicate superior performance of Vienna model for each data sets and both year of 2011 and 2012.

Moreover, a cumulative distribution of the percentages of the results for different relative error bins is demonstrated in Figure 4-18.

Table 4-2. Vienna model performance using different data sets

Year	Weather Data	MBE	MAE	RMSE	CV (RMSE)	MeAPE	MeBE	R ²
2011	BPI	-0.63	31.49	47.75	31.52	13.85	-0.01	0.77
	Hohe Warte	-4.01	30.97	48.92	36.36	13.11	0.001	0.74
2012	BPI	-0.06	32.92	48.65	30.05	13.80	-0.01	0.77
	Hohe Warte	-3.98	27.91	43.46	32.13	11.77	0.002	0.78

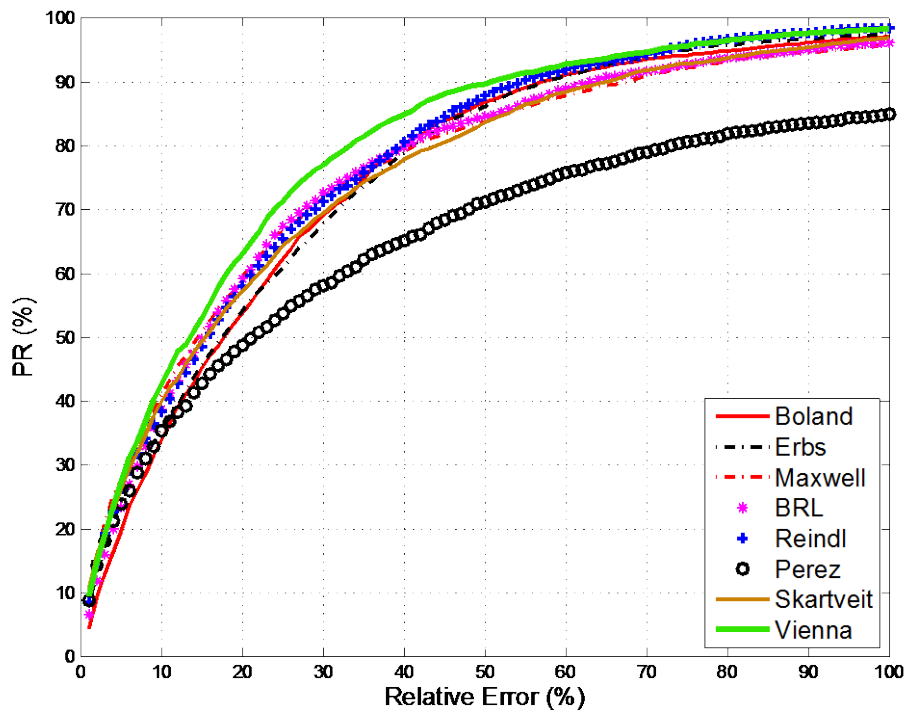


Figure 4-18. The cumulative distribution function (CDF) of the relative errors for all models (BPI data 2011)

4.5 Radiance model performance

In order to evaluate model performance for clear sky, a number of statistical measures, namely mean bias error MBE, Root mean square error RMSE and coefficient of variation of RMSE, have been considered (See *Table 4-3*). Results indicate that with increase of patch altitude, the performance of the models worsens. Main reason for that can be a decrease in the number of patches within each ring by increasing patch altitudes. Moreover, predicted radiance coefficients using by the new model versus measured radiance coefficient by sky scanner were compared (See pages 45 to 50).

Table 4-3. Values of statistical measures for RC functions

<i>Patch altitude</i>	MBE	RMSE	CV(RMSE)
6°	3.95e-05	0.0331	20.3
18°	8.45e-05	0.0885	22.7
30°	-8.16-04	0.1747	27.7
42°	-0.0022	0.2017	31.2
54°	1.44e-04	0.2516	35.7
66°	6.61-04	0.2541	36.1
78°	1.11e-04	0.2125	32.0
87°	0.0094	0.3465	37.1

Results & Discussions

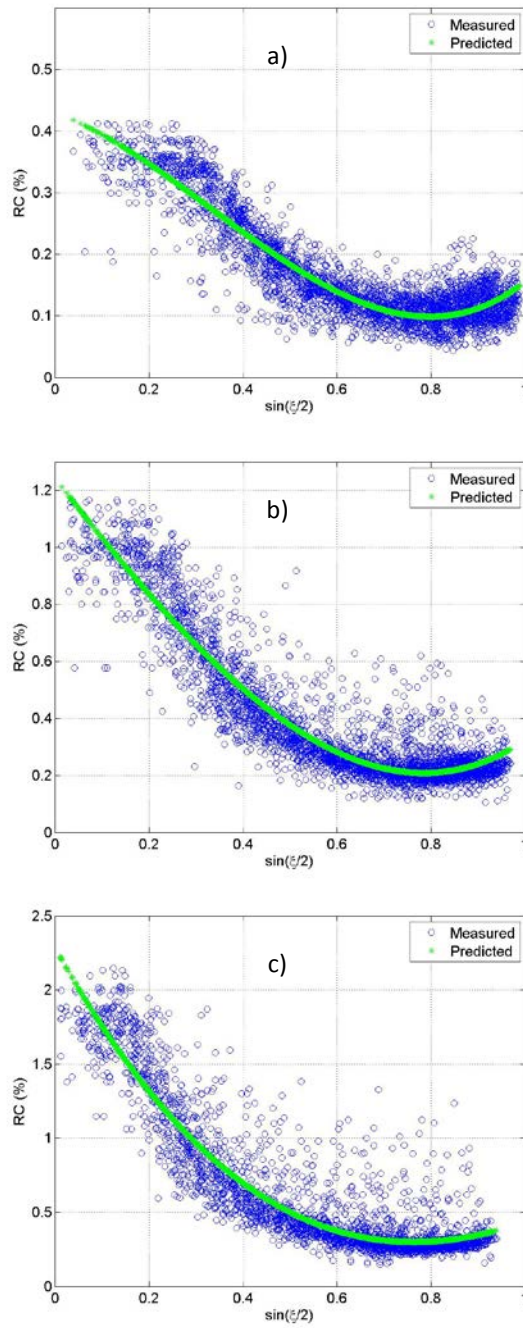


Figure 4-19. Best Cubic polynomial function model (a) Patch altitude = 6° , b) Patch altitude = 18°, and c) Patch altitude = 30°

Results & Discussions

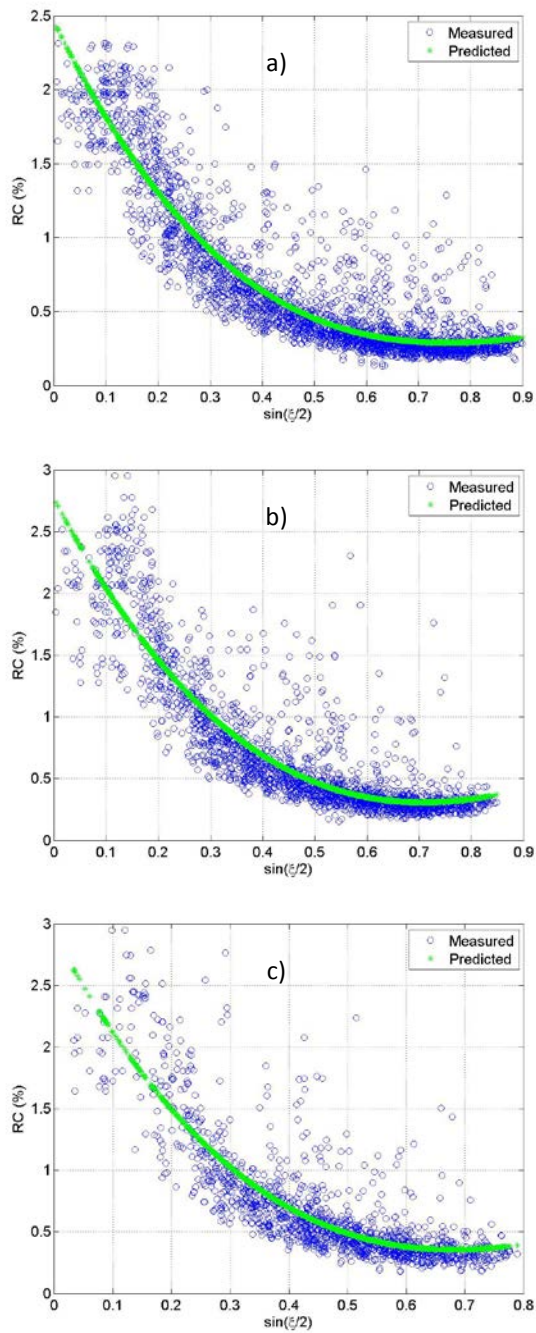


Figure 4-20. Best Cubic polynomial function model (a) Patch altitude = 42°, b) Patch altitude = 54°, and Patch altitude = 66°)

Results & Discussions

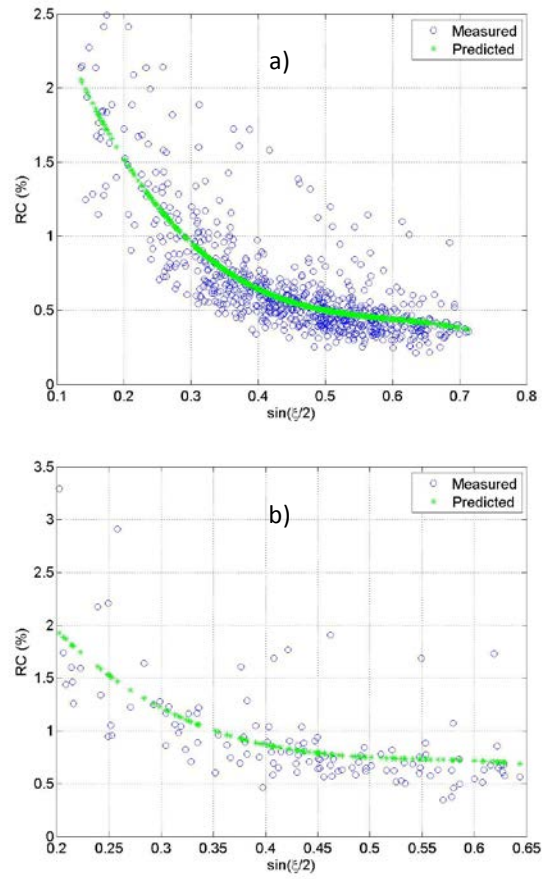


Figure 4-21. Best Cubic polynomial function model (a) Patch altitudes 78° and b) 87 degrees)

Results & Discussions

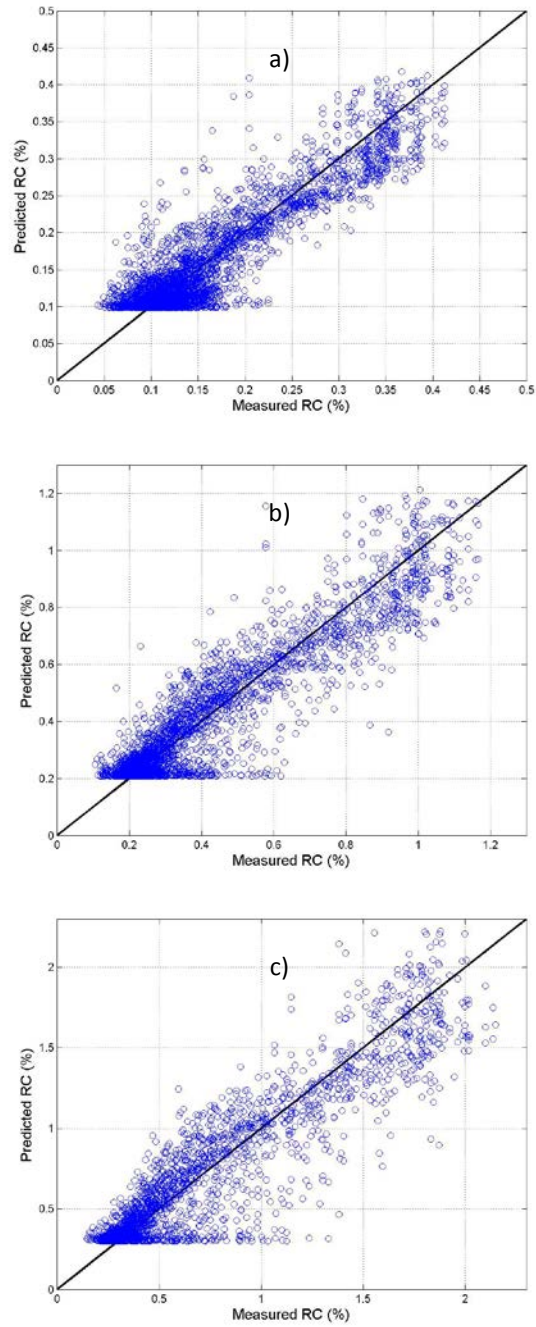


Figure 4-22. Comparison of measured RC versus Predicted (a) Patch altitude = 6°
, b) Patch altitude = 18°, and c) Patch altitude = 30°)

Results & Discussions

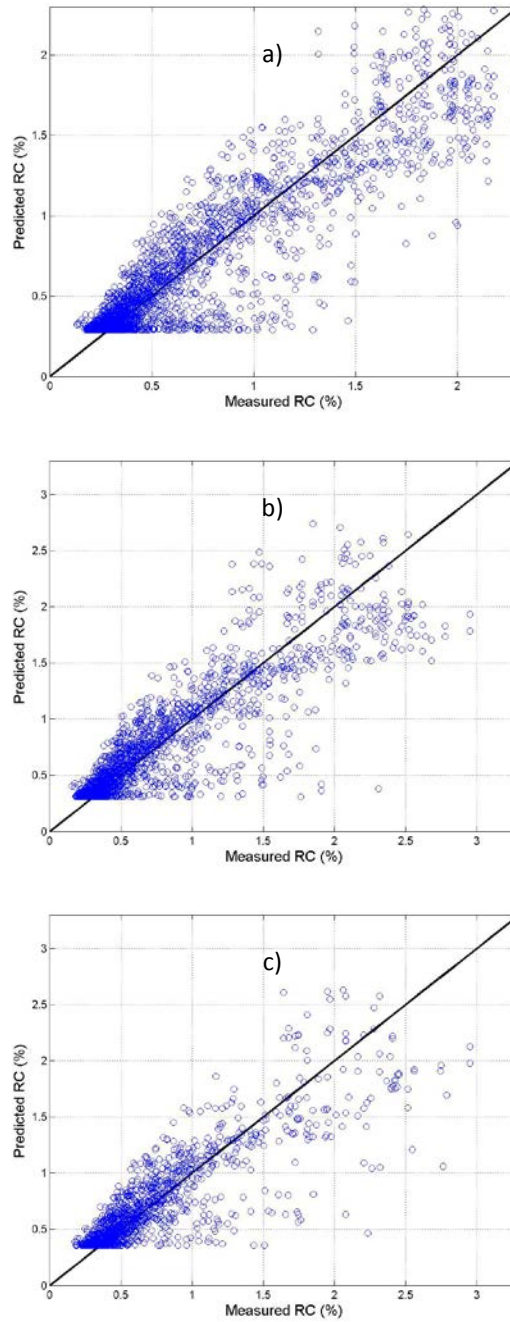
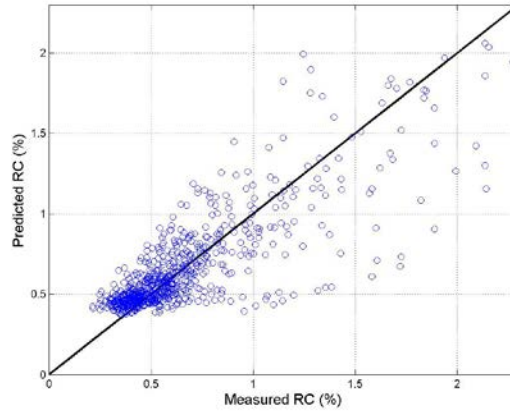
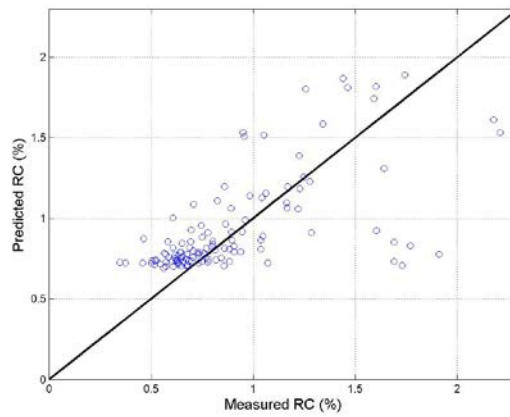


Figure 4-23. Comparison of measured RC versus Predicted (a) Patch altitude = 42°, b) Patch altitude = 54 , and Patch altitude = 66)

Results & Discussions



a)



b)

Figure 4-24. Comparison of measured RC versus Predicted (a) Patch altitudes 78 and b) 87 degrees)

Chapter 5

Conclusions and Outlook

5.1 Diffuse fraction models

Superior performance of Vienna model was indicated in Chapter 4. However, the resolution of Vienna model needs to be improved. This can be achieved by looking at additional data i.e. cloud cover, clouds' color etc. but crucial point to be considered is the limitation of weather data in many locations. This fact may put an end to efforts for development of more accurate diffuse component prediction model.

Further studies will be done regarding the clouds impact. Appendix II, recommends a new approach for developing a satisfactory global model.

5.2 Radiance distribution model

Radiance distribution on each point of the sky dome over the clear sky is a function of angular distance of the point and sun (See Chapter 4, Radiance model performance). Clouds will add to complexity of the model. The location and quantity of the clouds can significantly influence the radiance of a point. Therefore, getting those data requires additional meteorological information i.e. cloud cover, satellite meteorological map, which are not easy accessible. Consequently, generation of an accurate model requires better understanding of cloud formation and behavior, by looking at the wind information other variables such as variability hours introduced by Skartveit and Olseth (1998).

Chapter 6

References

6.1 Literature

- Boland J. Scott, L. Luther, M. 2001. *Modeling the diffuse fraction of global solar radiation on a horizontal surface*. *Environmetric*, 12:103-116.
- Davies J.A., McKay, D.C., Luciani, G. and Abdel-Wahab, M. 1988. *Validation of models for estimating solar radiation on horizontal surfaces*. Downsview, Ontario : IEA-SHCP TaskIX Final Report.
- Dervishi, S. Mahdavi, A. 2012. *Computing diffuse fraction of global horizontal solar radiation: A model comparison*. *Solar Energy*, Vol. 86 1796–1802.
- Erbs D.G. Klein, S.A. and Duffie J.A. 1982. *Estimation of the diffuse radiation fraction for hourly, daily and monthly-average global radiation*. *Solar Energy*, Vol. 28. pp. 293-302.
- European Commission: *Health Effects of Artificial Light*. Scientific Committee on Emerging and Newly Identified Health Risks (SCENIHR) Adopted by the SCENIHR during the 17th plenary meeting of 19 March 2012s
- Iqbal M . 1980. *Prediction of hourly diffuse solar radiation from measured hourly global solar radiation on a horizontal surface*. *Solar Energy*, Vol. 24. - pp. 491-03.
- Iqbal, M. 1983. *Introduction to solar radiation, Academic*. Toronto, Canada.
- Lapillonne, B. Sebi, C. Pollier, K. Mairet, N. 2012. *Energy Efficiency Trends in Buildings in the EU*. ODYSSEE MURE project. supported by Intelligent Energy Europe. ADEME editions: Paris

References

- Lauret P. Boland, J. Ridley, B. 2010. *Derivation of a solar diffuse fraction model in a bayesian framework*. Case Studies in Business, Industry and Government Statistics 1, Vol. 3 pp: 108-122.
- Liu, B.Y.H., Jordan, R.C., (1960). *The interrelationship and characteristic distribution of direct, diffuse and total solar radiation*. Solar Energy 4:1-19.
- Maxwell, E. L. 1987. *A quasi-physical model for converting hourly global horizontal to direct normal insolation*. Report SERI/TR-215-3087, Solar Energy Institute, Golden, CO.
- Orgill J.F. Hollands, K.G. 1977. *Correlation equation for hourly diffuse radiation on a horizontal surface*. Solar Energy, Vol. 19. pp. 357-359.
- Parmerlee G, V. 1954. *Irradiation of Vertical and horizontal surfaces by diffuse solar radiation from cloudless skies*. ASHVE transaction. pp. 341-358.
- Perez R. Seals, R. Zelenka, A. and Ineichen, P. 1990a. *Climatic evaluation of models that predict hourly direct irradiance from hourly global irradiance: Prospects for performance improvements*. Solar Energy, Vol. 44, 99-108.
- Perez R. Ineichen, P. Seals, R. Michalsky, J. Stewart, R. 1990b. *Modeling daylight availability and irradiance components from direct and global irradiance*. Solar Energy, Vol. 44. pp. 271-289.
- Perez R. Ineichen, P. Maxwell, E. Seals, R. Zelenka, A. 1991. *Dynamic global-to-direct irradiance conversion models*. ISES Solar World Congress, Denver USA, pages 951-956.
- Reindl, D.T., Beckman, W.A., Duffie, J.A. 1990. *Diffuse fraction correlations*. Solar Energy, Vol. 45(1) p:1-7.
- Skartveit, A. Olseth, J.A. 1987. *A model for the diffuse fraction of hourly global radiation*. Solar Energy, 38:271-274.
- Skartveit, A. Olseth, J.A. Tuft, M.E. 1998. *An hourly diffuse fraction model with correction for variability and surface albedo*. Solar Energy, 63(3):173-183.
- Spencer, JW. 1982. *A comparison of methods for estimating hourly diffuse solar radiation from global solar radiation*. Solar Energy Vol. 29. - pp. 19-32.

References

Vazifeh, E. Dervishi, S. Mahdavi, A. 2013. *Calculation models for the diffuse fraction of global solar radiation*. CESBP Conference, Vienna, Austria. 587-590.

Zentralanstalt für meteorologie und geodynamik. 1971-2000. Klimadaten von Österreich. <http://www.zamg.ac.at/cms/de/aktuell>.

U.S. Energy Information Administration (EIA). *Annual energy outlook 2014*. 2011 and 2012 degree days based on state-level data from the National Oceanic and Atmospheric Administration's Climatic Data Center and Climate Prediction Center.

6.2 Tables

<i>Table 3-1. brief summary of models and their input variables</i>	7
<i>Table 3-2. Bins used in Perez function</i>	18
<i>Table 3-3. Bins used for the Perez second model</i>	18
<i>Table 3-4. Variables used in Vienna model</i>	19
<i>Table 3-5. parameters for the Vienna model</i>	26
<i>Table 3-6. Parameters of RC model functions for clear sky</i>	30
<i>Table 4-1. result of model comparison using mentioned statistical measures</i>	38
<i>Table 4-2. Vienna model performance using different data sets</i>	43
<i>Table 4-3. Values of statistical measures for RC functions</i>	44
<i>Table 6-1. Instruments specifications</i>	59
<i>Table 6-2. Recorded climate data for Vienna city from 1971 to 2000</i>	61
<i>Table 6-3. Perez Look-up Table</i>	65
<i>Table 6-4. azimuth difference vs. irradiance coeff. figure Index</i>	72

6.3 Figures

Figure 1-1. Typical energy usage of commercial buildings profile (U.S energy information administration) 2

Figure 1-2. Depiction of direct and diffuse component of solar insolation 2

Figure 2-1. Weather station overview 5

Figure 3-1. a) RMSE for predicted diffuse horizontal irradiance for each iteration b) R2 for predicted diffuse horizontal irradiance for each iteration 20

Figure 3-2. a) RMSE for predicted diffuse horizontal irradiance for each iteration b) R2 for predicted diffuse horizontal irradiance for each iteration 21

Figure 3-3. a) RMSE for predicted diffuse horizontal irradiance for each iteration b) R2 for predicted diffuse horizontal irradiance for each iteration 22

Figure 3-4. a) RMSE for predicted diffuse horizontal irradiance for each iteration b) R2 for predicted diffuse horizontal irradiance for each iteration 23

Figure 3-5. a) RMSE for predicted diffuse horizontal irradiance for each iteration b) R2 for predicted diffuse horizontal irradiance for each iteration 24

Figure 3-6. a) RMSE for predicted diffuse horizontal irradiance for each iteration b) R2 for predicted diffuse horizontal irradiance for each iteration 25

Figure 3-7. Correlation of Radiance Coefficient versus angular distance between sun disk and patch center under all weather conditions 27

Figure 3-8. Correlation of Radiance Coefficient versus angular distance between sun disk and patch center (Clear days) 27

Figure 3-9. Radiance coefficients for each ring versus sinus of half angular distance between patch center and sun disk (a) Patch altitude = 6°, b) Patch altitude = 18°, and c) Patch altitude = 30°) 28

Figure 3-10. Radiance coefficients for each ring versus sinus of half angular distance between patch center and sun disk (a) Patch altitude = 42°, b) Patch altitude = 54°, and c) Patch altitude = 66°) 29

Figure 3-11. Radiance coefficients for each ring versus sinus of half angular distance between patch center and sun disk (Patch altitude = 78) 30

Figure 4-1. Schema for the models implementation and evaluation process 31

Figure 4-2. Comparison of Erbs et al. (1982) diffuse fraction model with measured data (year 2012) 32

Figure 4-3. Comparison of Reindl (1987) diffuse fraction model with measured data (year 2012) 33

Figure 4-4. Comparison of Skartveit and Olseth (1998) diffuse fraction model with measured data (year 2012) 33

References

<i>Figure 4-5. Comparison of Boland (2001) diffuse fraction model with measured data (year 2012)</i>	34
<i>Figure 4-6. Comparison of BRL (2010) diffuse fraction model with measured data (year 2012)</i>	35
<i>Figure 4-7. Comparison of Maxwell (1987) diffuse fraction model with measured data (year 2012)</i>	35
<i>Figure 4-8. Comparison of Perez (1991) diffuse fraction model with measured data (year</i>	36
<i>Figure 4-9. Comparison of Vienna (2013) diffuse fraction model with measured data (year 2012)</i>	36
<i>Figure 4-10. Comparison of Vienna (2013) diffuse fraction model with measured data (year 2012)</i>	36
<i>Figure 4-11. Bar graphs for statistical measures (BPI data set)</i>	39
<i>Figure 4-12. RMSE of models for each range of clearness Index and percentage of data for each range (BPI data 2011)</i>	39
<i>Figure 4-13. R-square of models for each range of clearness Index and percentage of data for each range (BPI data 2011)</i>	40
<i>Figure 4-14. The cumulative distribution function (CDF) of the relative errors for all models (BPI data 2012)</i>	40
<i>Figure 4-15. Impact of solar altitude on fraction of diffuse radiation (BPI data 2011)</i>	41
<i>Figure 4-16. Impact of solar time on diffuse radiation (BPI data 2011)</i>	41
<i>Figure 4-17. Season impact on diffuse radiation (BPI data 2011)</i>	42
<i>Figure 4-18. The cumulative distribution function (CDF) of the relative errors for all models (BPI data 2011)</i>	43
<i>Figure 4-19. Best Cubic polynomial function model (a) Patch altitude = 6°</i>	45
<i>Figure 4-20. Best Cubic polynomial function model (a) Patch altitude = 42°, b) Patch altitude = 54°, and Patch altitude = 66°</i>	46
<i>Figure 4-21. Best Cubic polynomial function model (a) Patch altitudes 78° and b) 87 degrees)</i>	47
<i>Figure 4-22. Comparison of measured RC versus Predicted (a) Patch altitude = 6°</i>	48
<i>Figure 4-23. Comparison of measured RC versus Predicted (a) Patch altitude = 42°, b) Patch altitude = 54, and Patch altitude = 66)</i>	49
<i>Figure 4-24. Comparison of measured RC versus Predicted (a) Patch altitudes 78 and b) 87 degrees)</i>	50
<i>Figure 6-1. illustration of BPI and Hohe Warte microclimatic observatory weather station (Source: Vienna city map http://www.wien.gv.at/stadtplan/)</i>	58
<i>Figure 6-2. Fisheye camera captures of sky dome with k_t higher than 0.8</i>	62
<i>Figure 6-3. k_t and Global irradiance variation for a sunny day observed by Fisheye camera (10th of July 2011)</i>	63
<i>Figure 6-4. Comparison of Cloudless clearness index</i>	64

Appendix A: Weather Station

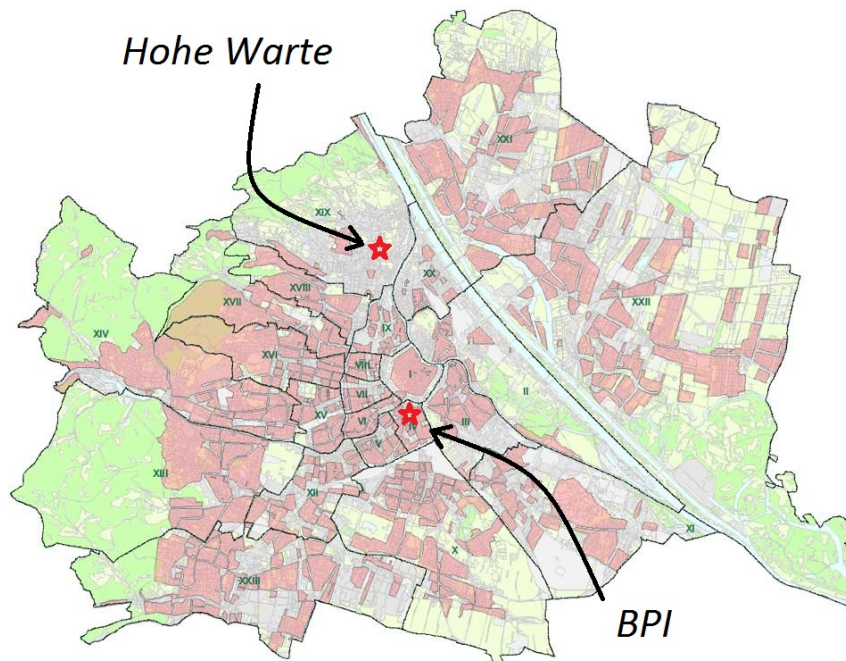
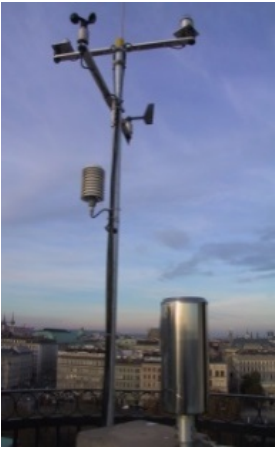



Figure 6-1. illustration of BPI and Hohe Warte microclimatic observatory weather station (Source: Vienna city map <http://www.wien.gv.at/stadtplan/>)

The microclimatic observatory weather station of Building physics and building ecology department is located on the rooftop of Technical university of Vienna, at the heart of Vienna city, Austria. Some of the specifications of the equipment have been demonstrated below:

Table 6-1. Instruments specifications

Weather station	Specifications
	<p>Outdoor air temperature: Absolute Error: < 0.3 K; Temperature range: -30 to +70 ° C; Response time < 20 s (≥ 1.5 m/s)</p> <p>Outdoor relative humidity: Absolute Error < $\pm 2\%$; Humidity range 0 to 100 %; Response time < 10 s (≥ 1.5 m/s)</p> <p>Global horizontal illuminance: Absolute Error < 5%; Illuminance range 0 - 50 000 lx</p> <p>Wind speed: Absolute Error: < 1%; Wind speed range 0 - 75 m.s⁻¹</p>
Sunshine Pyranometer (SPN1)	Specifications
	<p>Global irradiance (horizontal and vertical): Range 0 -1300 W.m⁻²; Spectral range 380 nm-2800 nm; Temperature range -20 to +60 ° C ; Accuracy Cosine Correction < 3% ; Linearity: < 1% , Absolute Error: < 10%</p> <p>Diffuse irradiance (Sunshine pyranometer SPN1): Overall accuracy $\pm 5\%$; Daily integrals $\pm 5\% \pm 10$ W.m⁻²; Hourly averages $\pm 8\% \pm 10$ W.m⁻²; Resolution 0.6 W. m⁻²=0.6 mV; Range 0 to > 2000 W. m⁻²; Analogue output sensitivity 1mv= 1 W. m⁻²; Analogue output range: 0-2500 mV; Temperature range -20 to +70 ° C; Accuracy Cosine Correction $\pm 2\%$ of incoming radiation over 0-90° zenith angle; Accuracy azimuth angle $\pm 5\%$ over 360° rotation; Response time < 200 ms</p> <p>Sunshine status threshold: 120</p>

		W.m ⁻² in the direct beam
Pyranometer (GSM 10.7)		Specifications
		Global irradiance (horizontal and vertical): Range: 0 -1300 W.m ⁻² ; Spectral range 380 nm-2800 nm; Temperature range -20 to +60 ° C; Accuracy cosine correction <3%; Linearity <1%; Absolute Error <10%
Sky scanner (MS321LR)		Specifications
 http://eko-usa.com/		Luminance: Sensitivity 50 kcd.m ⁻² ; Resolution 15 cd.m ⁻² ; Entire sky scanning time: 4 min/145 points , resolution (angle): 0.0036°, accuracy (angle): 0.2° Radiance: sensitivity: 300 W.m ⁻² .sr ⁻¹ , resolution: 1.0 W.m ⁻² .sr ⁻¹ , entire sky scanning time: 4 min/145 points , resolution (angle): 0.0036°, accuracy (angle): 0.2°
Fisheye camera (LMK 98-4)		Specifications
		Luminance: Standard resolution 1380 x 1030 Pixel; Higher resolution 2448 x 2050 Pixel, 4008 x 2672 Pixel, 4008 x 4008 Pixel; Resolution (dynamic) Single picture measurement: 1:1100 (~ 61 dB); Multi picture measurement: 1:3600 (~ 71 dB); High Dynamic measurement 1:10000000 (~140 dB); A/D conversion 12/14 Bit; Measurement time from 1 to 15 sec for different luminance values depending on adjusted exposure time; Accuracy: DL < 3 % (for standard illuminant A); D _{x,y} < 0.0020 (for standard illuminant A)

Appendix

Table 6-2. Recorded climate data for Vienna city from 1971 to 2000

	Jan	Feb	Mar	Apr	May	Jun	Jul	Aug	Sep	Oct	Nov	Dec	Year
Rec. Hi °C	16.7	19.1	25.5	27.8	30.7	35.9	36	37	31.1	26.4	20.8	16.1	37
Avg. Hi °C	2.9	5.1	10.3	15.2	20.5	23.4	25.6	25.4	20.3	14.2	7.5	4	14.5
Daily Avg. °C	0.1	1.6	5.7	10	15.2	18.2	20.2	19.8	15.3	9.9	4.6	1.5	10.2
Avg. L °C	-2.0	-0.9	2.4	5.8	10.5	13.5	15.4	15.3	11.7	7	2.4	-0.5	6.7
Rec. L °C	-19.6	-17.2	-15.3	-2.7	1	4.8	8.4	7	3.1	-4.5	-9.6	-18.1	-19.6
PP. mm	37.2	39.4	46.1	51.7	61.8	70.2	68.2	57.8	53.5	40	50	44.4	620.3
SF cm	18.6	15.6	8.3	1.5	0	0	0	0	0	0	7.9	16.4	68.3
APD ¹	7.3	7.6	8.3	7.5	8.5	9.1	9	8	7	6	8.3	8.2	94.8
ASD ²	13.9	10	4	0.4	0	0	0	0	0	0	2.7	8.3	39.3
MSSH ³	60.9	90.1	131.5	173.8	228	222.8	241.8	239.2	167.6	131.2	65.5	52	1804.4

¹ Average precipitation days

² Average snowy days

³ Monthly sunshine hours

Appendix B: The ratio of hourly global horizontal radiation to hourly extraterrestrial radiation

High amount for k_t occurs with the unshaded sun and part of clouds in the sky. The clouds contribute to the increase of diffuse component and unobstructed sun contributes to direct beam radiation. Sum of diffuse and direct beam radiation will result into high amount of global radiation or k_t . This phenomenon has been mentioned by several authors, Orgill and Hollands 1977, Erbs et al. 1982, Skartveit and Olseth 1987. Reindl et al. 1990 indicated that along with the increase of k_t , under condition of clear sky, solar altitude becomes the dominant predictor variable. Reindl (1990) also assumed that sky cloudiness decreases with the increase of k_t .

Figure 6-2, shows 6 random fisheye camera false color images of the sky, which has k_t of higher than 0.8. Clear part of the sky is colored with green hue. Red and orange hues show the cloudy part; bright part of the sky and yellow hue is approximately the sun disc. As it has been demonstrated, none of the sky conditions represents clear sky within this range of high amount of k_t .

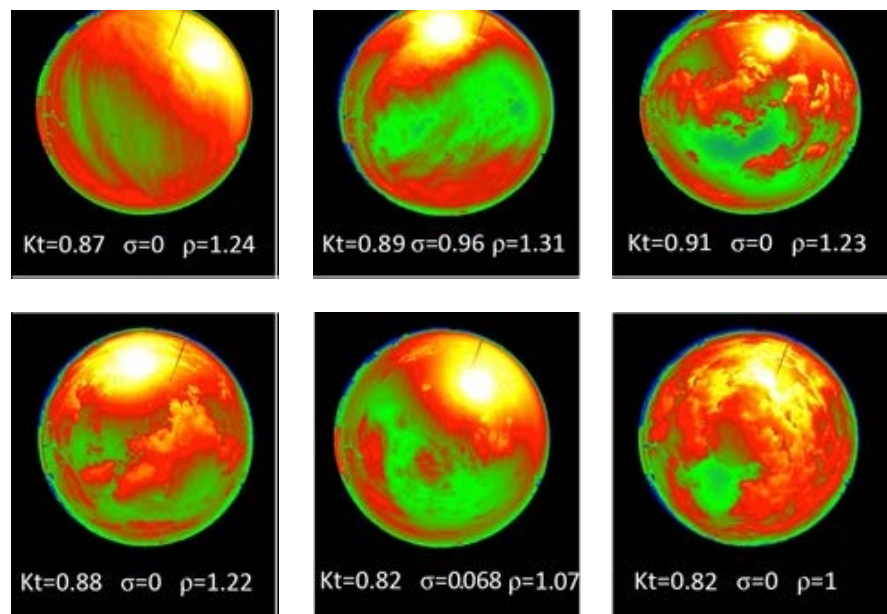


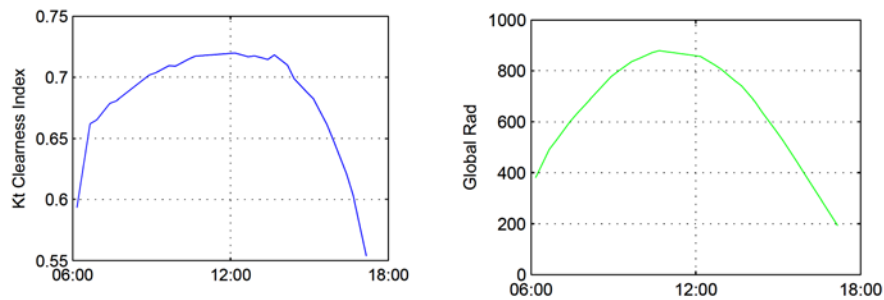
Figure 6-2. Fisheye camera captures of sky dome with k_t higher than 0.8

Figure 6-3, illustrates variation of k_t and global horizontal irradiance under the condition of a sunny summer day (10th July 2011, Vienna), observed by fisheye camera of BPI weather station. k_t varies between 0.55 to 0.7. Several authors, as well as Maxwell 1987 and Skartveit and Olseth 1998, derived an equation using air mass and solar altitude as a variable respectively. In this work using a number of measurement data under the clear sky condition, an attempt was made by the author to predict cloudless clearness index k_c using air mass. Predicted k_c , is found to be:

$$k_c = -2.425 \times 10^{-16} e^{7.474m_{air}} + 0.801e^{-0.099m_{air}} \quad (65)$$

Amount of k_c was compared with the Maxwell and Skartveit cloudless clearness index. Results indicate that for a number of sunsets and sunrises, k_c predicts negative values (See Figure 6-4-a). Besides, both Maxwell and Skartveit correlations overestimate clearness index for cloudless skies of Vienna (See Figure 6-4-b). As a conclusion, it has been suggested by the author to use 90% of Skartveit cloudless clearness index in order to calculate k_c :

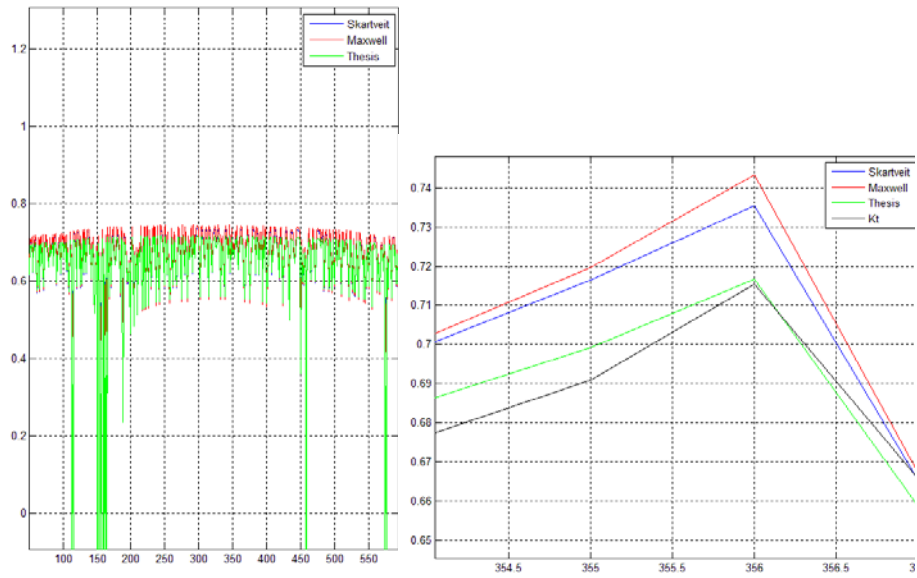
$$k_c = 0.9(0.83 - 0.56e^{-0.06\alpha}) \quad (66)$$



a) k_t variation through a clear day

b) GHI through a clear day

Figure 6-3. k_t and Global irradiance variation for a sunny day observed by Fisheye camera (10th of July 2011)



a) Comparison of cloudless clearness index

b) Comparison of cloudless clearness index (sunny day sample)

Figure 6-4. Comparison of Cloudless clearness index

Appendix C: Perez look-up table

Perez look-up table consists of 252 rows and 6 columns, where each array is a coefficient to be multiplied by Maxwell DISC beam irradiance. In order to derive the coefficient for each time step, four insolation condition parameters must be calculated, which are adjusted Clearness index (K'_t) that represents meteorologically similar conditions irrespective of the position of the sun. Z is the solar zenith angle, $\Delta K'_t$ stability index and W as atmospheric precipitable water (See *Table 3-2*). With all these information, the index of Perez coefficient within the matrix can be calculated with the suggested formula:

$Bin_{K'_t}$ = number of bin in the *Table 3-2* for the range of K'_t

Bin_Z = number of bin in the *Table 3-2* for the range of Z

$Bin_{\Delta K'_t}$ = number of bin in the *Table 3-2* for the range of $\Delta K'_t$

Bin_W = number of bin in the *Table 3-2* for the range of W

Finally:

Row's number = $((Bin_Z - 1) * 6 + Bin_{K'_t}) * 6 + Bin_{\Delta K'_t}$

Column's number = Bin_W

Table 6-3. Perez Look-up Table

Row number	Column number	1	2	3	4	5
1	1	0.38523	0.38523	0.38523	0.46288	0.31744
2	2	0.33839	0.33839	0.22127	0.31673	0.50365
3	3	0.23568	0.23568	0.24128	0.15783	0.26944
4	4	0.83013	0.83013	0.17197	0.84107	0.45737
5	5	0.54801	0.54801	0.478	0.96688	1.03637
6	6	0.54801	0.54801	1	3.01237	1.97654
7	7	0.58269	0.58269	0.22972	0.89271	0.56995
8	1	0.13128	0.13128	0.38546	0.51107	0.12794
9	2	0.22371	0.22371	0.19356	0.30456	0.19394
10	3	0.22997	0.22997	0.27502	0.31273	0.24461
11	4	0.0901	0.18458	0.2605	0.68748	0.57944
12	5	0.13153	0.13153	0.37019	1.38035	1.05227

Appendix

13	6	1.11625	1.11625	0.92803	3.52549	2.31692
14	7	0.0901	0.237	0.30004	0.81247	0.66497
15	1	0.58751	0.13	0.4	0.53721	0.83249
16	2	0.30621	0.12983	0.20446	0.5	0.68164
17	3	0.22402	0.26062	0.33408	0.50104	0.35047
18	4	0.42154	0.75397	0.75066	3.70684	0.98379
19	5	0.70668	0.37353	1.24567	0.86486	1.99263
20	6	4.8644	0.11739	0.26518	0.35918	3.31082
21	7	0.39208	0.49329	0.65156	1.93278	0.89873
22	1	0.12697	0.12697	0.12697	0.12697	0.12697
23	2	0.81082	0.81082	0.81082	0.81082	0.81082
24	3	3.24168	2.5	2.29144	2.29144	2.29144
25	4	4	3	2	0.97543	1.96557
26	5	12.49417	12.49417	8	5.08352	8.79239
27	6	21.74424	21.74424	21.74424	21.74424	21.74424
28	7	3.24168	12.49417	1.62076	1.37525	2.33162
29	1	0.12697	0.12697	0.12697	0.12697	0.12697
30	2	0.81082	0.81082	0.81082	0.81082	0.81082
31	3	3.24168	2.5	2.29144	2.29144	2.29144
32	4	4	3	2	0.97543	1.96557
33	5	12.49417	12.49417	8	5.08352	8.79239
34	6	21.74424	21.74424	21.74424	21.74424	21.74424
35	7	3.24168	12.49417	1.62076	1.37525	2.33162
36	1	0.12697	0.12697	0.12697	0.12697	0.12697
37	2	0.81082	0.81082	0.81082	0.81082	0.81082
38	3	3.24168	2.5	2.29144	2.29144	2.29144
39	4	4	3	2	0.97543	1.96557
40	5	12.49417	12.49417	8	5.08352	8.79239
41	6	21.74424	21.74424	21.74424	21.74424	21.74424
42	7	3.24168	12.49417	1.62076	1.37525	2.33162
43	1	0.33744	0.33744	0.96911	1.09719	1.11608
44	2	0.33744	0.33744	0.96911	1.11603	0.6239
45	3	0.33744	0.33744	1.53059	1.02442	0.90848
46	4	0.58404	0.58404	0.84725	0.91494	1.2893
47	5	0.33744	0.33744	0.31024	1.43502	1.85283
48	6	0.33744	0.33744	1.01501	1.09719	2.11723
49	7	0.33744	0.33744	0.96911	1.14573	1.4764
50	1	0.3	0.3	0.7	1.1	0.79694
51	2	0.21987	0.21987	0.52653	0.80961	0.6493
52	3	0.38665	0.38665	0.11932	0.57612	0.68546

Appendix

53	4	0.74673	0.39983	0.47097	0.98653	0.78537
54	5	0.57542	0.9367	1.6492	1.49584	1.33559
55	6	1.31967	4.00257	1.27639	2.64455	2.51867
56	7	0.66519	0.67891	1.01236	1.19994	0.98658
57	1	0.37887	0.97406	0.5	0.49188	0.66529
58	2	0.10521	0.26347	0.40704	0.55346	0.58259
59	3	0.3129	0.34524	1.14418	0.85479	0.61228
60	4	0.11907	0.36512	0.56052	0.79372	0.8026
61	5	0.78161	0.83739	1.27042	1.53798	1.29295
62	6	1.15229	1.15229	1.49208	1.24537	2.1771
63	7	0.42466	0.52955	0.96691	1.03346	0.95873
64	1	0.31059	0.71441	0.25245	0.5	0.6076
65	2	0.97519	0.36342	0.5	0.4	0.5028
66	3	0.17558	0.19625	0.47636	1.07247	0.49051
67	4	0.71928	0.69862	0.65777	1.19084	0.68111
68	5	0.42624	1.46484	0.67855	1.15773	0.97843
69	6	2.50112	1.78913	1.38709	2.39418	2.39418
70	7	0.49164	0.67761	0.68561	1.0824	0.73541
71	1	0.597	0.5	0.3	0.31005	0.41351
72	2	0.31479	0.33631	0.4	0.4	0.44246
73	3	0.16651	0.46044	0.55257	1	0.46161
74	4	0.40102	0.55911	0.40363	1.01671	0.67149
75	5	0.40036	0.75083	0.84264	1.8026	1.02383
76	6	3.3153	1.51038	2.44365	1.63882	2.13399
77	7	0.53079	0.74585	0.69305	1.45804	0.8045
78	1	0.597	0.5	0.3	0.31005	0.80092
79	2	0.31479	0.33631	0.4	0.4	0.23704
80	3	0.16651	0.46044	0.55257	1	0.58199
81	4	0.40102	0.55911	0.40363	1.01671	0.89857
82	5	0.40036	0.75083	0.84264	1.8026	3.40039
83	6	3.3153	1.51038	2.44365	1.63882	2.50878
84	7	0.20434	1.15774	2.00308	2.62208	1.40938
85	1	1.24221	1.24221	1.24221	1.24221	1.24221
86	2	0.05698	0.05698	0.65699	0.65699	0.92516
87	3	0.08909	0.08909	1.04043	1.23248	1.2053
88	4	1.05385	1.05385	1.39969	1.08464	1.23334
89	5	1.15154	1.15154	1.11829	1.53164	1.41184
90	6	1.49498	1.49498	1.7	1.80081	1.6716
91	7	1.01845	1.01845	1.1536	1.32189	1.29467
92	1	0.7	0.7	1.02346	0.7	0.94583

Appendix

93	2	0.8863	0.8863	1.33362	0.8	1.06662
94	3	0.90218	0.90218	0.95433	1.12669	1.09731
95	4	1.0953	1.07506	1.17649	1.13947	1.09611
96	5	1.20166	1.20166	1.4382	1.25628	1.19806
97	6	1.52585	1.52585	1.86916	1.98541	1.91159
98	7	1.28822	1.08281	1.28637	1.16617	1.11933
99	1	0.6	1.02991	0.85989	0.55	0.8136
100	2	0.60445	1.02991	0.85989	0.6567	0.92884
101	3	0.45585	0.75058	0.80493	0.823	0.911
102	4	0.52658	0.93231	0.90862	0.98352	0.98809
103	5	1.03611	1.10069	0.84838	1.03527	1.04238
104	6	1.04844	1.65272	0.9	2.35041	1.08295
105	7	0.81741	0.97616	0.8613	0.97478	1.00458
106	1	0.78211	0.56428	0.6	0.6	0.66574
107	2	0.89448	0.68073	0.54199	0.8	0.66914
108	3	0.48746	0.81895	0.84183	0.87254	0.70904
109	4	0.70931	0.87278	0.90848	0.95329	0.84435
110	5	0.86392	0.94777	0.87622	1.07875	0.93691
111	6	1.28035	0.86672	0.76979	1.07875	0.97513
112	7	0.72542	0.86997	0.86881	0.95119	0.82922
113	1	0.79175	0.65404	0.48317	0.409	0.59718
114	2	0.56614	0.94899	0.97182	0.65357	0.71855
115	3	0.64871	0.63773	0.87051	0.8606	0.6943
116	4	0.63763	0.76761	0.92567	0.99031	0.84767
117	5	0.73638	0.94606	1.11759	1.02934	0.94702
118	6	1.18097	0.85	1.05	0.95	0.88858
119	7	0.70056	0.80144	0.96197	0.90614	0.82388
120	1	0.5	0.5	0.58677	0.47055	0.62979
121	2	0.5	0.5	1.05622	1.26014	0.65814
122	3	0.5	0.5	0.63183	0.84262	0.58278
123	4	0.55471	0.73473	0.98582	0.91564	0.89826
124	5	0.71251	1.20599	0.90951	1.07826	0.88561
125	6	1.89926	1.55971	1	1.15	1.12039
126	7	0.65388	0.79312	0.90332	0.94407	0.79613
127	1	1	1	1.05	1.17038	1.17809
128	2	0.96058	0.96058	1.05953	1.17903	1.13169
129	3	0.87147	0.87147	0.99586	1.14191	1.1146
130	4	1.20159	1.20159	0.99361	1.10938	1.12632
131	5	1.06501	1.06501	0.82866	0.93997	1.01793
132	6	1.06501	1.06501	0.62369	1.11962	1.13226

Appendix

133	7	1.07157	1.07157	0.95807	1.11413	1.12711
134	1	0.95	0.97339	0.85252	1.0922	1.09659
135	2	0.80412	0.91387	0.98099	1.09458	1.04242
136	3	0.73754	0.93597	0.99994	1.05649	1.05006
137	4	1.03298	1.03454	0.96846	1.03208	1.01578
138	5	0.9	0.97721	0.94596	1.00884	0.96996
139	6	0.6	0.75	0.75	0.84471	0.8991
140	7	0.9268	0.96503	0.96852	1.04491	1.03231
141	1	0.85	1.02971	0.9611	1.05567	1.0097
142	2	0.81853	0.96001	0.99645	1.08197	1.03647
143	3	0.76538	0.9535	0.94826	1.05211	1.00014
144	4	0.77561	0.90961	0.9278	0.9878	0.9521
145	5	1.00099	0.88188	0.87595	0.9491	0.89369
146	6	0.90237	0.87596	0.80799	0.94241	0.91792
147	7	0.85658	0.92827	0.94682	1.03226	0.97299
148	1	0.75	0.85793	0.9838	1.05654	0.98024
149	2	0.75	0.98701	1.01373	1.13378	1.03825
150	3	0.8	0.94738	1.01238	1.09127	0.99984
151	4	0.8	0.91455	0.90857	0.99919	0.91523
152	5	0.77854	0.80059	0.79907	0.90218	0.85156
153	6	0.68019	0.31741	0.50768	0.38891	0.64671
154	7	0.79492	0.91278	0.96083	1.05711	0.94795
155	1	0.75	0.83389	0.86753	1.05989	0.93284
156	2	0.9797	0.97147	0.99551	1.06849	1.03015
157	3	0.85885	0.98792	1.04322	1.1087	1.0449
158	4	0.8024	0.95511	0.91166	1.04507	0.94447
159	5	0.88489	0.76621	0.88539	0.85907	0.81819
160	6	0.61568	0.7	0.85	0.62462	0.6693
161	7	0.83557	0.94615	0.97709	1.04935	0.97997
162	1	0.68922	0.8096	0.9	0.7895	0.85399
163	2	0.85466	0.85284	0.9382	0.92311	0.95501
164	3	0.9386	0.93298	1.01039	1.04395	1.04164
165	4	0.84362	0.9813	0.95159	0.9461	0.96633
166	5	0.69474	0.81469	0.57265	0.4	0.72683
167	6	0.21137	0.67178	0.41634	0.29729	0.49805
168	7	0.84354	0.88233	0.91176	0.89842	0.96021
169	1	1.05488	1.07521	1.06846	1.15337	1.06922
170	2	1	1.06222	1.01347	1.08817	1.0462
171	3	0.88509	0.99353	0.94259	1.05499	1.01274
172	4	0.92	0.95	0.97872	1.02028	0.98444

Appendix

173	5	0.85	0.9085	0.83994	0.98557	0.96218
174	6	0.8	0.8	0.81008	0.95	0.96155
175	7	1.03859	1.0632	1.03444	1.11278	1.0378
176	1	1.01761	1.02836	1.05896	1.13318	1.04562
177	2	0.92	0.99897	1.03359	1.08903	1.02206
178	3	0.91237	0.94993	0.97977	1.02042	0.98177
179	4	0.84716	0.9353	0.93054	0.95505	0.94656
180	5	0.88026	0.86711	0.87413	0.97265	0.88342
181	6	0.62715	0.62715	0.7	0.77407	0.84513
182	7	0.9737	1.00624	1.02619	1.07196	1.01724
183	1	1.02871	1.01757	1.0259	1.08179	1.02424
184	2	0.92498	0.9855	1.0141	1.09221	0.99961
185	3	0.82857	0.93492	0.99495	1.02459	0.94971
186	4	0.90081	0.90133	0.92883	0.97957	0.9131
187	5	0.76103	0.84515	0.80536	0.93679	0.85346
188	6	0.6264	0.54675	0.7305	0.85	0.68905
189	7	0.95763	0.98548	0.99179	1.05022	0.9879
190	1	0.99273	0.99388	1.01715	1.05912	1.01745
191	2	0.97561	0.98716	1.02682	1.07544	1.00725
192	3	0.87109	0.93319	0.97469	0.97984	0.95273
193	4	0.82875	0.86809	0.83492	0.90551	0.87153
194	5	0.78154	0.78247	0.76791	0.76414	0.79589
195	6	0.74346	0.69339	0.51487	0.63015	0.71566
196	7	0.93476	0.95787	0.95964	0.97251	0.98164
197	1	0.96584	0.94124	0.9871	1.02254	1.01116
198	2	0.98863	0.99477	0.97659	0.95	1.03484
199	3	0.9582	1.01808	0.97448	0.92	0.98987
200	4	0.81172	0.86909	0.81202	0.85	0.82105
201	5	0.68203	0.67948	0.63245	0.74658	0.73855
202	6	0.66829	0.44586	0.5	0.67892	0.69651
203	7	0.92694	0.95335	0.95905	0.87621	0.99149
204	1	0.94894	0.99776	0.85	0.82652	0.99847
205	2	1.01786	0.97	0.85	0.7	0.98856
206	3	1	0.95	0.85	0.60624	0.94726
207	4	1	0.74614	0.75174	0.59839	0.72523
208	5	0.92221	0.5	0.3768	0.51711	0.54863
209	6	0.5	0.45	0.42997	0.40449	0.53994
210	7	0.96043	0.88163	0.77564	0.59635	0.93768
211	1	1.03	1.04	1	1	1.04951
212	2	1.05	0.99	0.99	0.95	0.99653

Appendix

213	3	1.05	0.99	0.99	0.82	0.97194
214	4	1.05	0.79	0.88	0.82	0.95184
215	5	1	0.53	0.44	0.71	0.92873
216	6	0.54	0.47	0.5	0.55	0.77395
217	7	1.03827	0.92018	0.91093	0.82114	1.03456
218	1	1.04102	0.99752	0.9616	1	1.03578
219	2	0.94803	0.98	0.9	0.95036	0.97746
220	3	0.95	0.97725	0.86927	0.8	0.95168
221	4	0.95187	0.85	0.74877	0.7	0.88385
222	5	0.9	0.82319	0.72745	0.6	0.83987
223	6	0.85	0.80502	0.69231	0.5	0.78841
224	7	1.01009	0.89527	0.77303	0.81628	1.01168
225	1	1.02245	1.0046	0.98365	1	1.03294
226	2	0.94396	0.99924	0.98392	0.90599	0.97815
227	3	0.93624	0.94648	0.85	0.85	0.93032
228	4	0.81642	0.885	0.64495	0.81765	0.86531
229	5	0.74296	0.76569	0.56152	0.7	0.82714
230	6	0.64387	0.59671	0.47446	0.6	0.6512
231	7	0.97174	0.94056	0.71488	0.86438	1.00165
232	1	0.99526	0.97701	1	1	1.03525
233	2	0.93981	0.97525	0.93998	0.95	0.98255
234	3	0.87687	0.87944	0.85	0.9	0.91781
235	4	0.87348	0.87345	0.75147	0.85	0.86304
236	5	0.76147	0.70236	0.63877	0.75	0.78312
237	6	0.73408	0.65	0.6	0.65	0.71566
238	7	0.94216	0.9191	0.77034	0.73117	0.99518
239	1	0.95256	0.91678	0.92	0.9	1.00588
240	2	0.92862	0.99442	0.9	0.9	0.98372
241	3	0.91307	0.85	0.85	0.8	0.92428
242	4	0.86809	0.80717	0.82355	0.6	0.84452
243	5	0.76957	0.71987	0.65	0.55	0.7335
244	6	0.58025	0.65	0.6	0.5	0.62885
245	7	0.90477	0.85265	0.70837	0.49373	0.94903
246	1	0.91197	0.8	0.8	0.8	0.95632
247	2	0.91262	0.68261	0.75	0.7	0.95011
248	3	0.65345	0.65933	0.7	0.6	0.85611
249	4	0.64844	0.6	0.64112	0.5	0.69578
250	5	0.57	0.55	0.5988	0.4	0.56015
251	6	0.47523	0.5	0.51864	0.33997	0.52023
252	7	0.74344	0.59219	0.60306	0.31693	0.79439

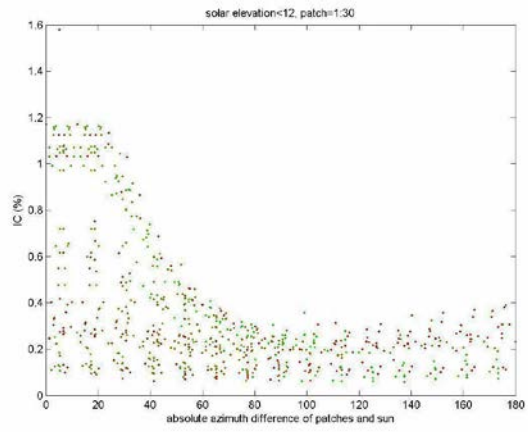
Appendix D: Irradiance distribution sheets

In order to have a better understanding of irradiance distribution in the sky dome correlation of azimuth difference between sun disk and patch center against irradiance coefficient has been plotted (See page 74 to 92). In *Table 6-4*, indices for mentioned figures are printed.

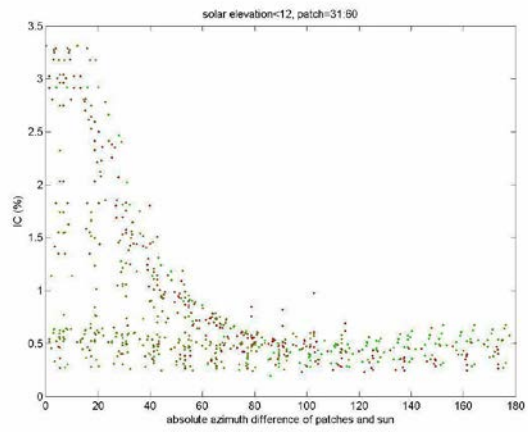
Table 6-4. azimuth difference vs. irradiance coeff. figure Index

Solar altitude	Patch: 1 : 30	Patch: 31 : 60	Patch: 61 : 84	Patch: 85:108	Patch: 109 : 126	Patch: 127 : 138
$0 < \alpha < 12$	A-1	A-2	A-3	A-4	A-5	A-6
$12 < \alpha < 24$	B-1	B-2	B-3	B-4	B-5	B-6
$24 < \alpha < 36$	C-1	C-2	C-3	C-4	C-5	C-6
$36 < \alpha < 48$	D-1	D-2	D-3	D-4	D-5	D-6
$\alpha > 48$	E-1	E-2	E-3	E-4	E-5	E-6

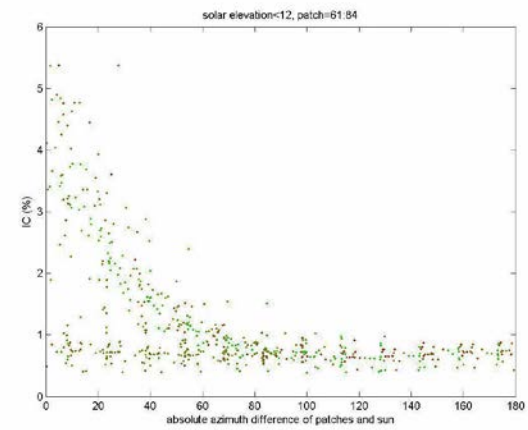
A1)



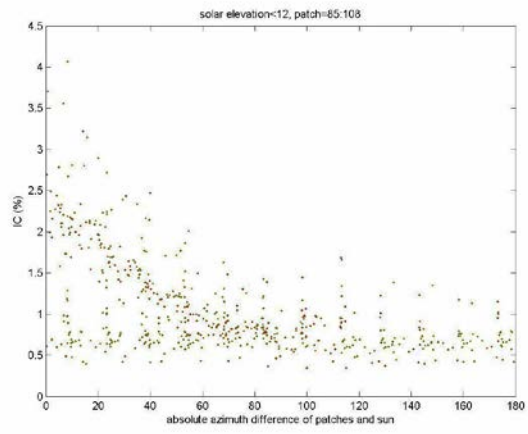
A2)



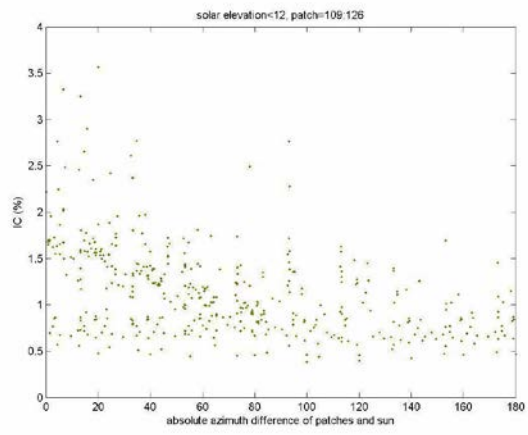
A3)



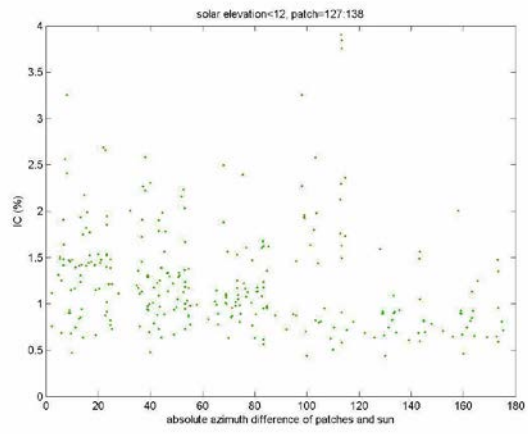
A4)



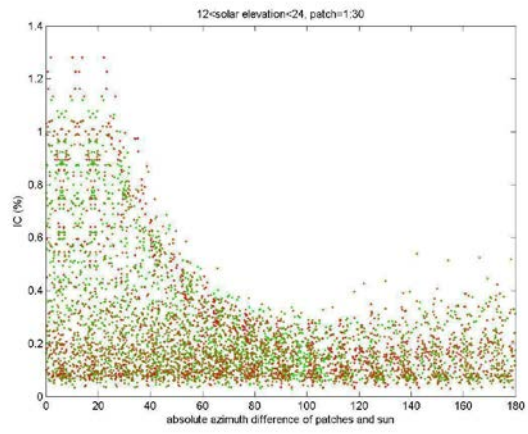
A5)



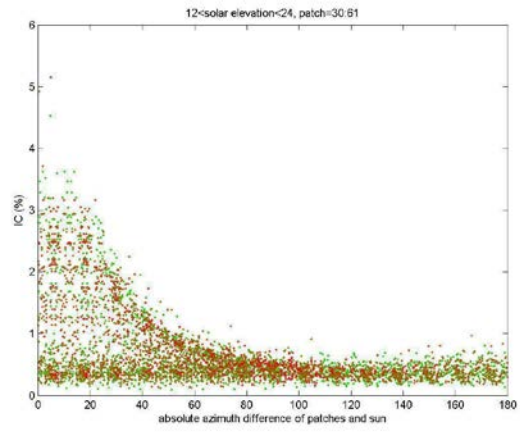
A6)



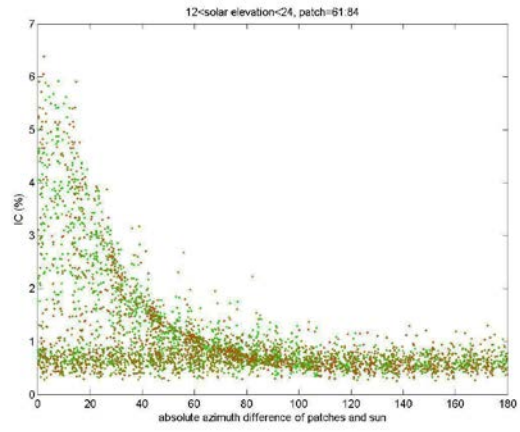
B1)



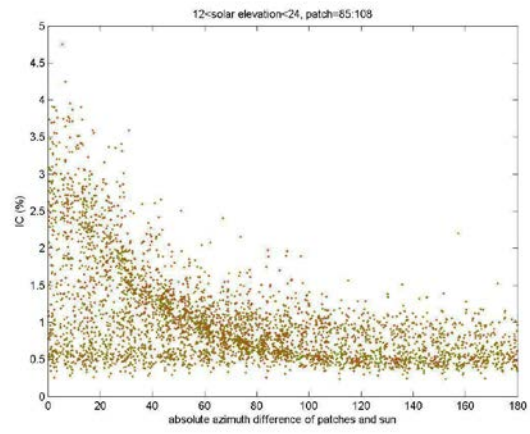
B2)



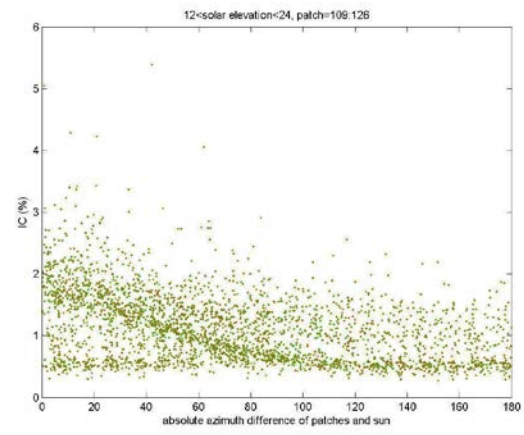
B3)



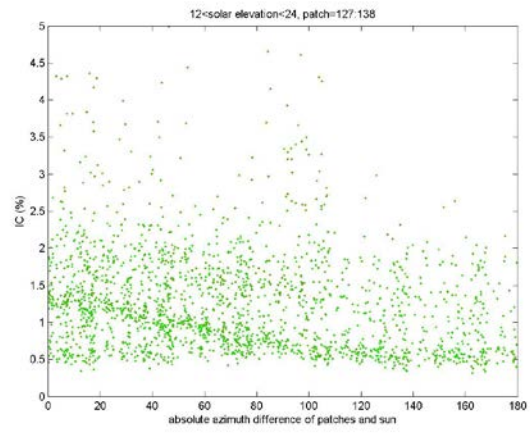
B4)



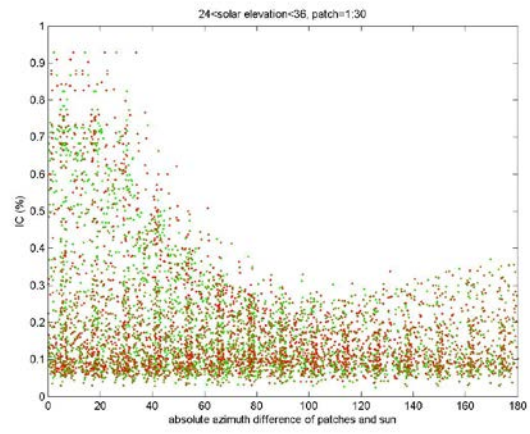
B5)



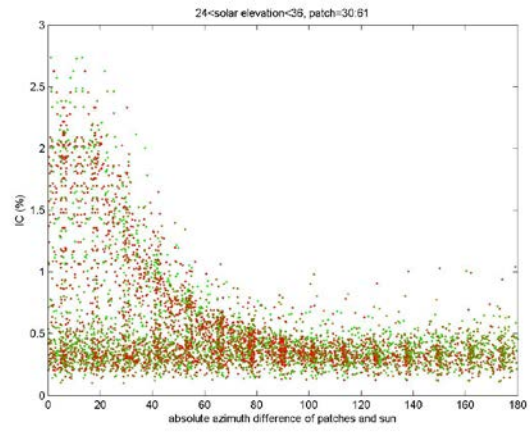
B6)



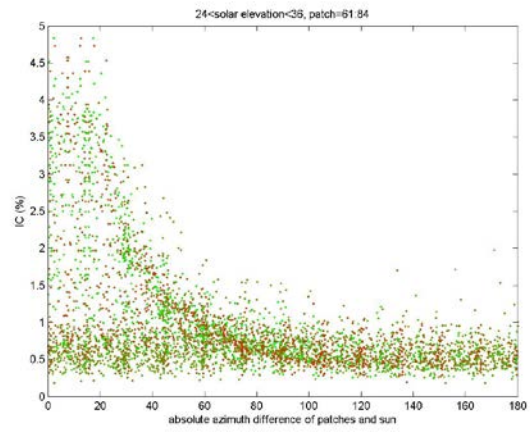
C1)



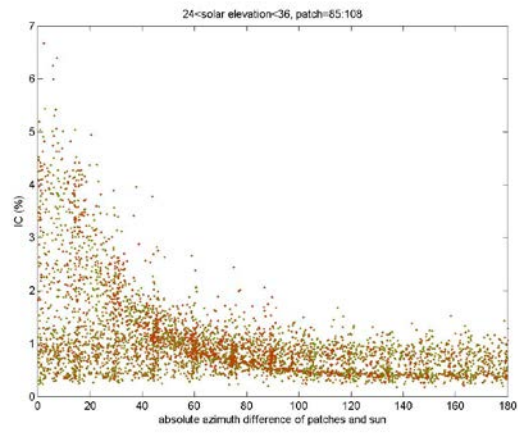
C2)



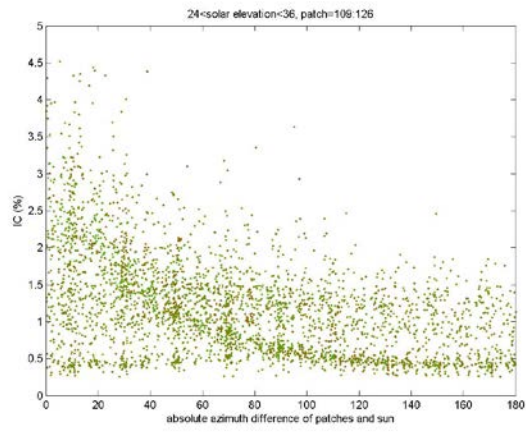
C3)



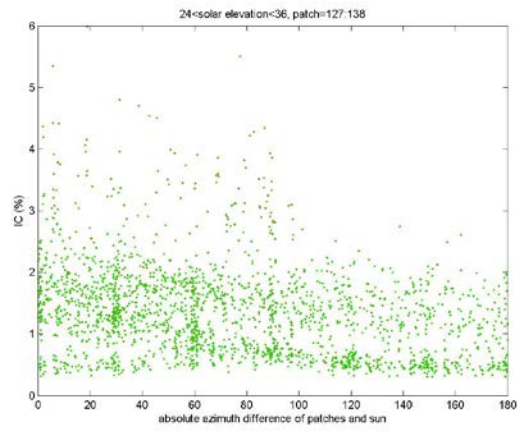
C4)



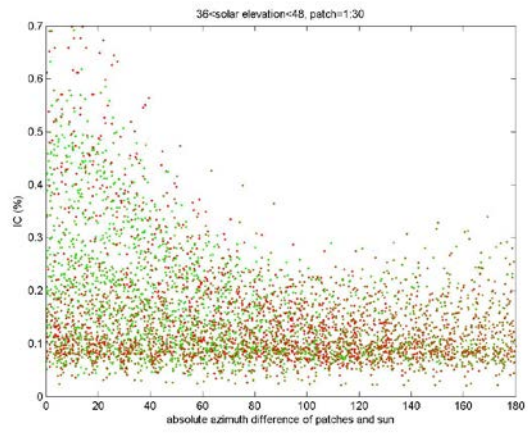
C5)



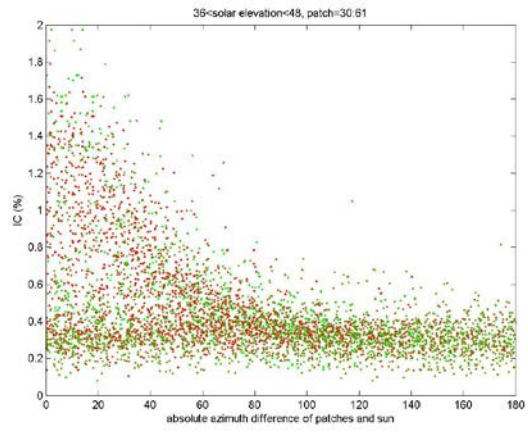
C6)



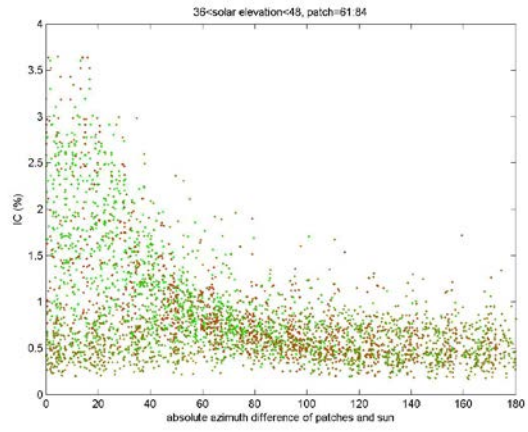
D1)



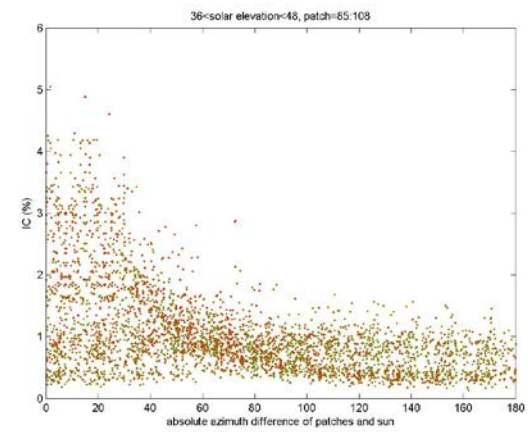
D2)



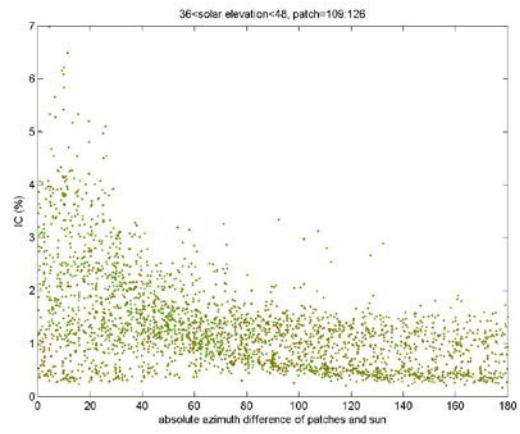
D3)



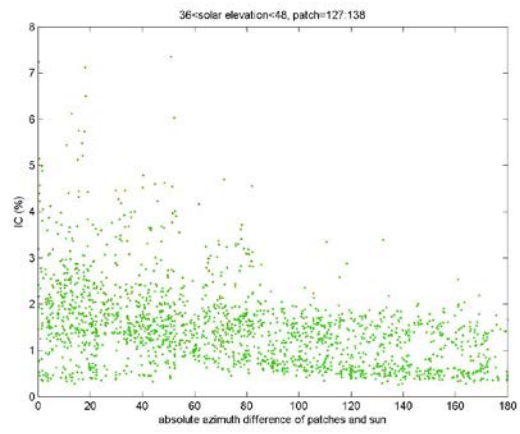
D4)



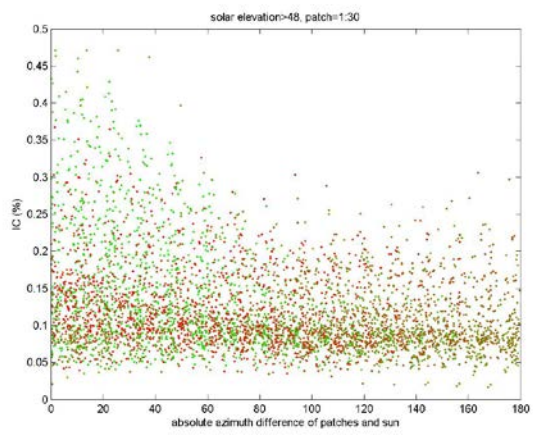
D5)



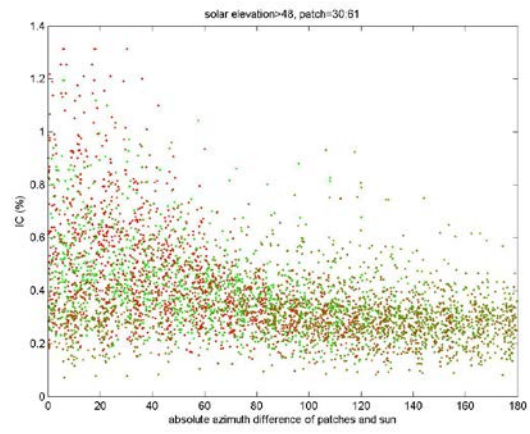
D6)



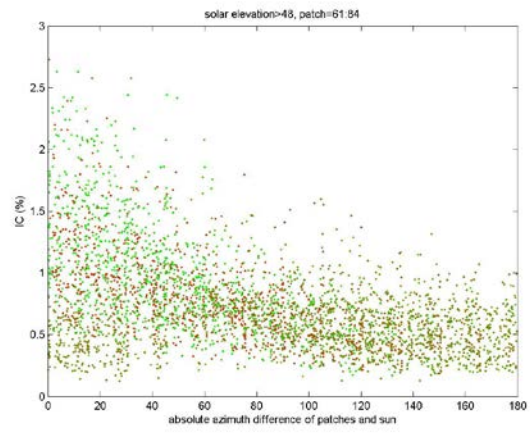
E1)



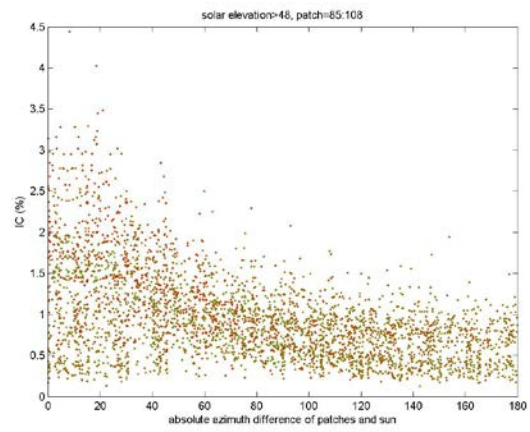
E2)



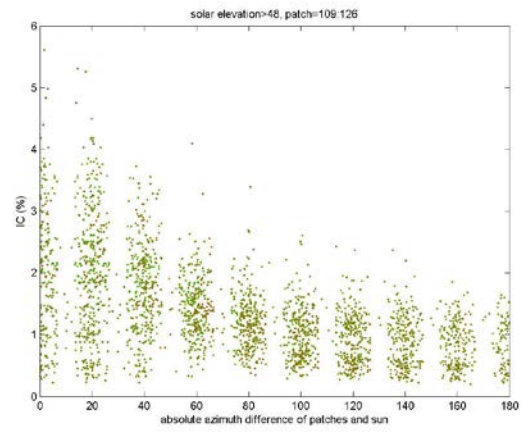
E3)



E4)



E5)



E6)

